Comparison of High Aspect Ratio Cooling Channel Designs for a Rocket Combustion Chamber With Development of an Optimized Design

Mary F. Wadel
Lewis Research Center, Cleveland, Ohio

The NASA STI Program Office ... in Profile

Since its founding, NASA has been dedicated to the advancement of aeronautics and space science. The NASA Scientific and Technical Information (STI) Program Office plays a key part in helping NASA maintain this important role.

The NASA STI Program Office is operated by Langley Research Center, the lead center for NASA's scientific and technical information. The NASA STI Program Office provides access to the NASA STI Database, the largest collection of aeronautical and space science STI in the world. The Program Office is also NASA's institutional mechanism for disseminating the results of its research and development activities. These results are published by NASA in the NASA STI Report Series, which includes the following report types:

- TECHNICAL PUBLICATION. Reports of completed research or a major significant phase of research that present the results of NASA programs and include extensive data or theoretical analysis. Includes compilations of significant scientific and technical data and information deemed to be of continuing reference value. NASA counter-part of peer reviewed formal professional papers, but having less stringent limitations on manuscript length and extent of graphic presentations.

- TECHNICAL MEMORANDUM. Scientific and technical findings that are preliminary or of specialized interest, e.g., quick release reports, working papers, and bibliographies that contain minimal annotation. Does not contain extensive analysis.

- CONTRACTOR REPORT. Scientific and technical findings by NASA-sponsored contractors and grantees.

- CONFERENCE PUBLICATION. Collected papers from scientific and technical conferences, symposia, seminars, or other meetings sponsored or co-sponsored by NASA.

- SPECIAL PUBLICATION. Scientific, technical, or historical information from NASA programs, projects, and missions, often concerned with subjects having substantial public interest.

- TECHNICAL TRANSLATION. English-language translations of foreign scientific and technical material pertinent to NASA's mission.

Specialized services that help round out the STI Program Office's diverse offerings include creating custom thesauri, building customized databases, organizing and publishing research results ... even providing videos.

For more information about the NASA STI Program Office, you can:

- Access the NASA STI Program Home Page at http://www.sti.nasa.gov/ STI-homepage.html

- E-mail your question via the Internet to help@sti.nasa.gov

- Fax your question to the NASA Access Help Desk at (301) 621-0134

- Phone the NASA Access Help Desk at (301) 621-0390

- Write to:
  NASA Access Help Desk
  NASA Center for AeroSpace Information
  800 Elkridge Landing Road
  Linthicum Heights, MD 21090-2934

Comparison of High Aspect Ratio Cooling Channel Designs for a Rocket Combustion Chamber With Development of an Optimized Design

Mary F. Wadel
Lewis Research Center, Cleveland, Ohio

National Aeronautics and
Space Administration

Lewis Research Center

Available from

COMPARISON OF HIGH ASPECT RATIO COOLING CHANNEL DESIGNS
FOR A ROCKET COMBUSTION CHAMBER WITH DEVELOPMENT
OF AN OPTIMIZED DESIGN

Abstract

by

MARY F. WADEL

An analytical investigation on the effect of high aspect ratio (height/width) cooling channels, considering different coolant channel designs, on hot-gas-side wall temperature and coolant pressure drop for a liquid hydrogen cooled rocket combustion chamber, was performed. Coolant channel design elements considered were; length of combustion chamber in which high aspect ratio cooling was applied, number of coolant channels, and coolant channel shape. Seven coolant channel designs were investigated using a coupling of the Rocket Thermal Evaluation code and the Two-Dimensional Kinetics code. Initially, each coolant channel design was developed, without consideration for fabrication, to reduce the hot-gas-side wall temperature from a given conventional cooling channel baseline. These designs produced hot-gas-side wall temperature reductions up to 22 percent, with coolant pressure drop increases as low as 7.5 percent from the baseline. Fabrication constraints for milled channels were applied to the seven designs. These produced hot-gas-side wall temperature reductions of up to 20 percent, with coolant pressure drop increases as low as 2 percent. Using high aspect ratio cooling channels for the entire length of the combustion chamber had no additional benefit on hot-gas-side wall temperature over using high aspect ratio cooling channels only in the throat region, but increased coolant pressure drop 33 percent. Independent of coolant channel shape, high aspect ratio cooling was able to reduce the hot-gas-side wall temperature by at least 8 percent, with as low as a 2 percent increase in coolant pressure

drop. The design with the highest overall benefit to hot-gas-side wall temperature and minimal coolant pressure drop increase was the design which used bifurcated cooling channels and high aspect ratio cooling in the throat region. An optimized bifurcated high aspect ratio cooling channel design was developed which reduced the hot-gas-side wall temperature by 18 percent and reduced the coolant pressure drop by 4 percent. Reductions of coolant mass flow rate of up to 40 percent were possible before the hot-gas-side wall temperature reached that of the baseline. At this reduced mass flow rate, the coolant pressure drop was reduced by 47 percent from the design value of 100 percent mass flow rate.

Table of Contents

Nomenclature

A_C total coolant flow area

C_C coolant side correlation coefficient

C_G hot-gas-side correlation coefficient

C_P specific heat

d_C coolant channel hydraulic diameter

d_G combustion chamber diameter

e   coolant channel surface roughness

f   friction factor

g_c gravitational constant, 32.2 ft·lb_m/lb_f·s^2

h   heat transfer coefficient

i   enthalpy

k   thermal conductivity

$\dot{m}$ mass flow

n   axial location n

N   total number of coolant channels

Nu   Nusselt number

Pr   Prandtl number

q   heat flux

$R_{cur.}$ radius of curvature

Re   Reynolds number

r_C coolant channel hydraulic radius

T   temperature

T_b bulk coolant temperature

T_w coolant wall temperature

t   coolant channel rib thickness

V   velocity

W   weight flow

ΔP pressure drop

ΔS length of coolant channel between two axial locations

ε_r coolant channel rib effectiveness

μ dynamic viscosity

π pi

ρ density

$\phi_{cur.}$ Coolant side curvature effect correction factor

$\phi_{ent.}$ Coolant side entrance effect correction factor

Subscripts

A   adiabatic

C   coolant

f   friction or viscous

G   hot-gas

M   momentum

S   static

W   wall

X   reference

1. Introduction

Among the many engineering challenges of reusable rocket engines is the need for chamber liners which will withstand the harsh combustion environment for many thermal cycles before failure. This is generally accomplished with a regenerative cooling system. In order to maintain chamber life, the cooling must keep the hot-gas-side wall temperature (T_{GW}) well below the material's melting limit. One solution to this problem is the use of high aspect ratio (height/width) cooling channels (HARCC).

Subscale and validation experiments at NASA Lewis Research Center have shown HARCC to significantly reduce the T_{GW} for the same pressure drop or with a modest pressure drop increase.[1,2] These tests also showed that HARCC and a decreased coolant mass flow rate could reduce the coolant pressure drop and still achieve a modest reduction in the T_{GW}. These experiments were conducted with bifurcated coolant channels, which had a high aspect ratio in the throat region.

HARCC has been experimentally investigated, but past analytical study has been limited. Previously, computer capabilities limited analytical study due to the need for super computing capability and large computing times. Advances in computer technology now make codes able to run in much shorter times using workstations. Investigation into the appropriate way to apply high aspect ratio cooling can now be done in relatively short periods of time with multiple iterations.

This analytical study investigated the effect of HARCC, considering different coolant channel designs, on T_{GW} and coolant channel pressure drop for a liquid hydrogen (LH$_2$) cooled rocket combustion chamber. The analytical method used here was validated with data from previous experimental results.[2] The combustion chamber configuration used was based upon the combustion chamber used to perform these experimental tests. Seven coolant channel designs were developed which varied the elements

of; the chamber length in which HARCC was applied, the number of coolant channels, and coolant channel shape. For this study, each of the seven coolant channel designs was initially developed, without consideration for fabrication, to reduce the maximum T_{GW} to 667 K (1200 °R) from a given conventional cooling channel baseline temperature profile with a maximum T_{GW} of 778 K (1400 °R). After these designs were determined, the seven coolant channel designs were modified to reflect current fabrication techniques. The seven designs were then evaluated to obtain an overall design, which had the most benefit to T_{GW} without significant adverse impact on coolant pressure drop. Based upon the selected overall HARCC coolant channel design, a final optimized HARCC coolant channel design was developed, which met the fabrication criteria. This optimized design was then used to evaluate the effects of reducing coolant mass flow rate on T_{GW} and coolant pressure drop.

2. Background

In order for the combustion chamber of a rocket engine to survive the harsh combustion environment, some form of cooling must be used. Two types of cooling are possible, passive and active. Passive cooling is generally accomplished by radiative heat transfer or through the use of an ablative material. Active cooling is generally accomplished by running a coolant through cooling passages in the combustion chamber wall. This is typically referred to as regenerative cooling. Regenerative cooling poses a more difficult engineering problem, since the entire cooling system becomes more complex. This study focuses on one aspect of a regenerative cooling system, the cooling channels.

The cooling channels in a rocket combustion chamber are located within the combustion chamber wall itself. Conventional cooling channels have aspect ratios (height/width) of approximately 2 to 2.5. One modification to the cooling channels that is possible is to raise the cooling channel aspect ratio above four. Figure 1 shows a schematic of a combustion chamber with coolant channel examples of both conventional and high aspect ratios. Figure 2 is a picture of an actual combustion chamber liner after is has been milled with rectangular coolant channels, similar to those shown in the schematic of Figure 1. Following the milling process, the combustion chamber liner, and its cooling channels, would be closed out with another material to finish the combustion chamber wall. Figure 3 shows a rocket combustion chamber after it has been fabricated, including cooling manifolding and instrumentation.

The cooling channels in a rocket combustion chamber are separated by structural ribs, as shown in Figure 1 and Figure 2. These ribs, besides providing structural support to the combustion chamber and directing the flow along the chamber, act as

A-A: Conventional channels
AR = 2 (AR = h/w)
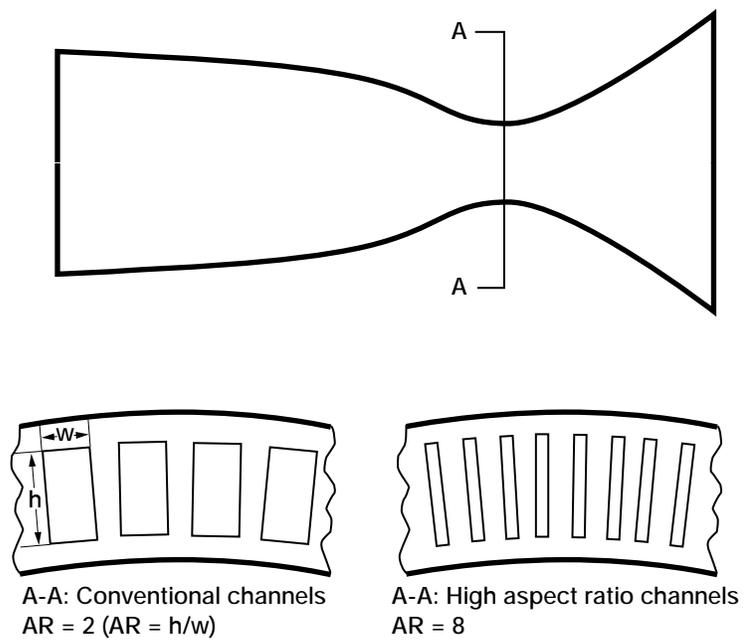
A-A: High aspect ratio channels
AR = 8

Figure 1.—Schematic of coolant channel cross-section comparing conventional aspect ratio channels to high aspect ratio channels.

Figure 2.—Combustion chamber liner after milling of bifurcated high aspect ratio cooling channels.

C-95-1783

Figure 3.—Combustion chamber after coolant channels have been closed out and fabrication has been completed.

extended surfaces for enhancing the heat transfer from the chamber liner to the coolant. This is similar to the fins in a classical heat exchanger.

If rib effectiveness is defined as the ratio of the heat transfer rate conducted through the base area of the rib to the heat transfer rate that would be convected through the same area without the rib, the rib can be evaluated for its ability to transfer heat from the combustion chamber liner to the coolant. Using the classical fin analysis from Incropera and DeWitt, [3] the rib effectiveness (ε_r) can be defined as:

$$\varepsilon_r = \left(\frac{2k}{ht}\right)^{1/2} \tag{1}$$

where k is the thermal conductivity of the rib material, h is the convective heat transfer coefficient, and t is the rib thickness. This equation has multiple assumptions, which, for simplicity, are: the heat transfer is one dimensional in the radial direction, the fluid temperature is uniform, and the convective heat transfer coefficient is constant along the rib-fluid interface. These assumptions do simplify the solution, but they allow for easier discussion of the heat transfer enhancement. Two other assumptions are that the rib thickness is much smaller than its axial length and the rib is infinitely high. An assumption that the rib is infinitely high is acceptable in this case. From a practical standpoint, there is an optimum rib height which provides nearly the same amount of heat transfer as that of an infinitely high rib. Above this optimum height, the fabrication constraints do not justify the minimum gains in heat transfer rate. Therefore, the optimum rib height is equivalent to an infinitely high rib.

Based upon the rib effectiveness equation given above, it can be seen that rib effectiveness can be increased by minimizing the rib thickness. However, decreasing the rib thickness decreases the rib base area, and limits heat transfer from the chamber

liner surface. Thus, to maximize the overall chamber liner heat transfer rate to the coolant, multiple, closely spaced, thin ribs are required. Using HARCC provides the opportunity to increase the coolant channel height, thereby extending the rib height. It also allows for more thin ribs to be placed closer together, while retaining the coolant flow area and the total base rib area. Therefore, HARCC provides the opportunity to greatly enhance the heat transfer rate between the chamber liner and the coolant.

Experimental investigation into the enhancement of the heat transfer rate by using HARCC has been accomplished at NASA Lewis Research Center.[1,2] These tests showed that HARCC could reduce the hot-gas-side wall temperature (T_{GW}) by as much as 25 percent, with minimal increases in the coolant channel pressure drop. This reduction in T_{GW} can increase the combustion chamber life and lower maintenance. Also, with lowered T_{GW}s, the maximum chamber performance can be achieved, since no film cooling of the combustion chamber is required. These tests also investigated reduced coolant mass flow rates, and the effect on the T_{GW} as well as pressure drop. Using HARCC and reducing the coolant mass flow rate still achieved a reduction in T_{GW}, and reduced the coolant pressure drop. However, these tests have been exclusively performed with bifurcated cooling channels. This analysis addressed the potential enhancement of the heat transfer rate using HARCC through different cooling channel geometries.

Previous experimental studies have investigated the effects of HARCC on T_{GW} and coolant pressure drop with reduced coolant mass flow rates.[1,2] Using reduced coolant mass flow rates in a rocket engine can offer many options for both the rocket engine cycle designer, as well as the thrust chamber and nozzle designer. Reduced coolant mass flow rates can reduce the requirements of high pressure pumping from turbopumps. They can also make the rocket engine combustion chamber and nozzle more flexible for

a particular design, thereby increasing the life of a particular combustion chamber design. This analysis addressed the effects of reduced coolant mass flow rates on the T_{GW} and coolant pressure drop for the selected overall HARCC design and the optimized HARCC design.

The effects of HARCC on a complete rocket engine system were not addressed in this analysis. The combustion chamber used in this analysis had a truncated nozzle, due to using the design for sea level testing. Therefore, the cooling channels were shorter than would potentially be used in an actual engine, and would not experience the same pressure drop or heat pick up, critical to some engine cycles. However, this does not alter the conclusions. The conclusions presented here are based upon a comparison with a baseline using the same combustion chamber and nozzle contour. If a full nozzle were to be considered for both the baseline and HARCC chambers, the comparative results and conclusions would be similar. The benefits of HARCC gained in a complete rocket engine system would need to be evaluated on an individual basis, relative to the specific engine cycle being considered. The focus of this analysis was on the effects of HARCC specific to the combustion chamber wall temperature and resultant coolant pressure drop.

3. Combustion Chamber Design

In order to make a comparison of the different HARCC designs, the thrust chamber contour selected, shown in Figure 4, was the one used for the previous HARCC validation experiments.[3,4] This contour was based on a 89 kN (20,000 lb$_f$) thrust chamber previously tested at NASA Lewis Research Center for thermal fatigue and new technology validation studies. The combustion chamber used an oxygen free electrical (OFE) copper inner liner with a nickel closeout structural jacket. The injector had 91 liquid oxygen (LOX) posts, and all fuel flowed through a porous-sintered-wire mesh face plate.
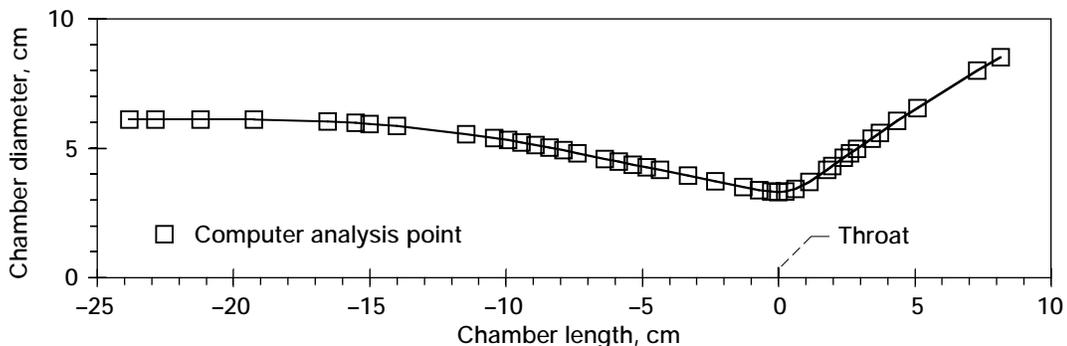
Figure 4.—Combustion chamber contour with RTE and TDK computer analysis points indicated.

The combustion chamber pressure used was 11 MPa (1600 psia) with a mixture ratio (oxygen/fuel) of 6.0. A rocket combustion analysis code (ROCCID) was used to obtain an axial profile of the mixture ratio in the combustion chamber upstream of the throat.[5] ROCCID is an injector analysis and design tool which predicts the effects of the injector upon combustion performance and stability based upon empirical data. LOX and gaseous hydrogen (GH$_2$) were used as propellants, with LH$_2$ as the coolant. The LOX mass flow rate used was 13.8 kg/sec (30.4 lb$_m$/sec), and the GH$_2$ mass flow rate

used was 2.3 kg/sec (5.1 lb_m/sec). The LH_2 mass flow rate was held constant for the initial design process at 2.3 kg/sec (5.1 lb_m/sec). Once an overall design was selected, the LH_2 mass flow rate was varied from 2.3 kg/sec (5.1 lb_m/sec) to 1.15 kg/sec (2.55 lb_m/sec) by 10 percent increments. The propellant and coolant inlet temperatures were assumed to be 91.7 K (165 °R) for LOX, 300 K (540 °R) for GH_2, and 44.4 K (80.0 °R) for LH_2.

4. Coolant Channel Design

4.1 Conventional Baseline Channel Design

In order to design the HARCC chambers to reduce T_{GW}, a baseline design with conventional coolant channels was used. This baseline design used 100 coolant channels at a conventional aspect ratio of 2.5. It had the same chamber contour and conditions as assumed for the HARCC designs. In an effort to make a comparison with the baseline, the total coolant channel area at a given axial location of the combustion chamber was kept the same between the baseline and the different designs. This coolant channel area constraint was removed, once an overall coolant channel geometry design was selected, in order to obtain a final optimized HARCC design.

4.2 Coolant Channel Designs

The three coolant channel design criteria considered were; the length of chamber in which HARCC was applied, the number of coolant channels, and coolant channel shape. Table I presents the seven different design combinations investigated.

Table I.—Matrix of Basic Coolant Channel Designs

Channel Shape	Number of Coolant Channels			Design
	Chamber Region	Throat Region	Nozzle Region	No.
Continuous	100[a]	100	100	1
	200	200	200	2
	100	100	100	3
	200	200	200	4
Bifurcated	100	200	100	5
Stepped	100	100	100	6
	200	200	200	7

[a]Shaded regions indicate areas of HARCC.

4.3 Coolant Channel Shape

The different coolant channel shapes considered were continuous, bifurcated, and stepped. Schematics for the different shapes are shown in Figure 5. All of the coolant channels were rectangular. Continuous channels were channels which had smooth transitions in width. Bifurcated channels were channels which were split into two channels and combined back to a single channel. Stepped channels were channels which made a sharp geometry change to another width.
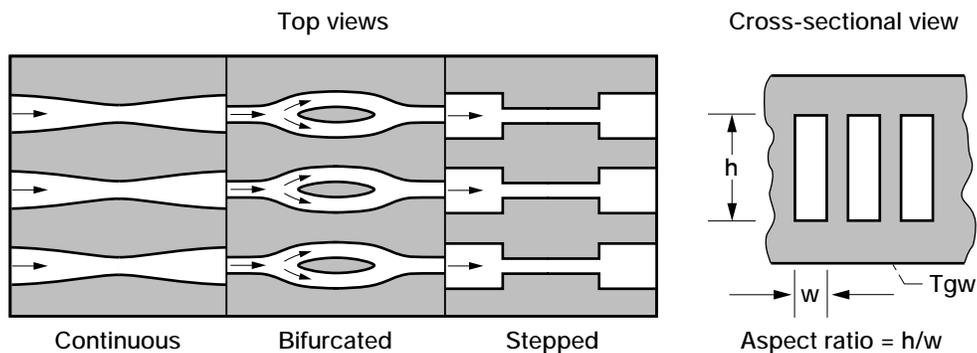
Figure 5.—Schematics of different coolant channel shapes evaluated.

4.4 Computer Codes

The designs were evaluated for their T_{GW} and coolant pressure drop using an iterative coupling between two different computer codes. The codes were a three dimensional rocket thermal evaluation code (RTE) and a nozzle analysis code, TDK, which uses an inviscid flow and boundary layer analysis technique.[6,7] For this study, RTE and TDK were coupled by iterating between heat transfer rate and T_{GW} in order to obtain the hot-gas side heat transfer. The following two sections are a discussion on the two computer codes individually, based upon the options used for this study. The third section discusses the coupling of the two codes.

4.4.1 RTE

RTE is a three-dimensional thermal analysis code for rocket combustion chambers.[6] RTE uses a three-dimensional finite difference technique to solve heat conduction equations in the wall involving iteration and axial marching. A Gauss-Seidel iterative method is used at each axial location evaluated to determine the wall temperature distributions both radially and circumferentially. When the axial march along the chamber is completed, the results are compared with the previous axial march until the convergence criteria are met. One section of a coolant channel is evaluated with the assumption that the combustion chamber is uniform circumferentially. Main inputs into RTE are the chamber and coolant channel geometries, propellant mixture ratio, propellant flow rates, combustion chamber pressure, and combustion chamber wall materials. The subroutines GASP (GAS Properties) and CET (complex Chemical Equilibrium and Transport properties) are used to determine the coolant and hot-gas side properties respectively.[8, 9, 10] Typical outputs from RTE are the temperature distribution of the combustion chamber wall, heat transfer rates, coolant and hot-gas side thermal properties, and coolant and hot-gas side transport properties. RTE is limited to combustion chambers which use rectangular coolant channels due to the formation of the finite difference grid. It also assumes a uniform coolant temperature in the coolant channels, at a given cross-sectional area. Additionally, RTE is limited to typical combustion chamber coolants, propellants, and materials.

The following is a discussion of the correlations used for the hot-gas side and coolant side heat transfer parameters for this study based upon the detailed discussion found in Ref. 6.

The hot-gas-side heat transfer for the RTE code is developed by calculating the heat transfer coefficient and the heat flux by the following:

$$h_{Gn} = \frac{C_{Gn} k_{GXn}}{d_{Gn}} Re_{GXn}^{0.8} Pr_{GXn}^{0.3} \tag{2}$$

and

$$q_n = \frac{h_{Gn}}{C_{pGXn}} \left(i_{GAWn} - i_{GWn} \right) \tag{3}$$

where C_G is the gas-side correlation coefficient, which is user input from empirical data.[11] Reynolds number and Prandtl number are defined as:

$$Re_{GXn} = \frac{4\dot{m}_G}{\pi d_{Gn} \mu_{GXn}} \frac{T_{GSn}}{T_{GXn}} \tag{4}$$

$$Pr_{GXn} = \frac{C_{pGXn} \mu_{GXn}}{k_{GXn}} \tag{5}$$

The coolant side heat transfer for the RTE code is evaluated for the side, top and bottom of the coolant channel, since the wall temperatures and heat flux around the coolant channel vary. The heat transfer calculations for the coolant side are developed by calculating the Nusselt number given by:

$$Nu_n = C_{Cn} Re_{CXn}^{0.8} Pr_{CXn}^{0.4} \phi_{ent.} \phi_{cur.} \tag{6}$$

where C_C is the coolant side correlation coefficient, which is user input from empirical data.[11,12] For this study, the value used was 0.023. Reynolds number and Prandtl number are defined as:

$$Re_{CXn} = Re_{CSn}\left(\frac{\rho_{CWn}}{\rho_{CSn}}\right)\left(\frac{\mu_{CSn}}{\mu_{CWn}}\right) \tag{7}$$

$$Pr_{CXn} = \frac{C_{pCXn}\mu_{CXn}}{k_{CXn}} \tag{8}$$

where Re_{CSn} is defined as:

$$Re_{CSn} = \frac{\dot{m}_C d_{Cn}}{A_{Cn}N_n\mu_{CSn}} \tag{9}$$

The terms $\phi_{ent.}$ and $\phi_{cur.}$ are added to account for the entrance effects of the coolant channel and the curvature effects of the coolant channel. They are defined as follows:[13,14]

$$\phi_{ent.} = \left[1 + \left(\frac{\sum_{i=1}^{n}\Delta S_{i,i} + 1}{d_{Cn}}\right)^{-0.7}\left(T_{Wn}/T_{bn}\right)^{0.1}\right] \tag{10}$$

$$\phi_{cur.} = \left[Re_{CXn}\left(\frac{r_{Cn}}{R_{cur.n}}\right)^2\right]^{\pm 1/20} \tag{11}$$

where d_C and r_C are the hydraulic diameter and radius of the coolant channel, respectively. The entrance effect ($\phi_{ent.}$) is calculated for a 90° bend, since the inlet of the coolant channels forms a 90° turn between the manifolding and the combustion chamber wall. The curvature effect ($\phi_{cur.}$) considers both the concave (+) and the convex (-) curvatures found in a typical rocket combustion chamber.

The Reynolds number for a combustion chamber coolant channel is in the turbulent flow region. Therefore, for the Reynolds number calculated in equation (6), an explicit form of the Colebrook equation, is used to account for the friction factor.[15] This is given by:

$$\frac{1}{\sqrt{f_n}} = -2.0 \log \left[\frac{e_n}{3.7065 d_{Cn}} - \frac{5.0452}{Re_{CXn}} \log \left(\frac{1}{2.8257} \left(\frac{e_n}{d_{Cn}} \right)^{1.1098} + \frac{5.8506}{Re_{CXn}^{0.8981}} \right) \right] \quad (12)$$

where straight tubes are assumed. To account for the effects of curvature, the friction factor is multiplied by Ito's correlation, given by:[16]

$$\phi_{cur.} = \left[Re_{CXn} \left(\frac{r_{Cn}}{R_{cur.n}} \right)^2 \right]^{1/20} \quad (13)$$

Pressure drop in the coolant channels is calculated for both the viscous and momentum effects. The viscous pressure drop is calculated using Darcy's law, and is given by:[17]

$$\left(\Delta P_{CSn-1,n} \right)_f = \frac{f_n}{8 g_c} \left(\frac{\rho_{CSm} + \rho_{CSn-1}}{d_{Cn} + d_{Cn-1}} \right) \left(V_{CSn} + V_{CSn-1} \right)^2 \Delta S_{n-1,n} \quad (14)$$

where :

$$V_{CSn} = \frac{\dot{m}_C}{\rho_{CSn} A_{Cn} N_n} \quad (15)$$

The momentum pressure drop is calculated using:

$$\left(\Delta P_{CSn-1,n}\right)_M = \left(\frac{2}{\left(NA_C\right)_{n-1} + \left(NA_C\right)_n}\right)\frac{W_C^2}{g_c}\left(\frac{1}{\left(\rho_{CS}A_CN\right)_n} - \frac{1}{\left(\rho_{CS}A_CN\right)_{n-1}}\right) \quad (16)$$

The viscous and momentum pressure drops are used to calculate the static pressures at each axial location. The RTE code is limited for evaluating the coolant pressure drop, since this method does not account for the effects of sudden area changes on the pressure drop with in the coolant channel. RTE also cannot account for variations in the coolant channels circumferentially. It assumes that the channels are uniform circumferentially.

4.4.2. TDK

TDK is used with RTE to determine the hot-gas side wall conditions with the consideration of a boundary layer in the combustion chamber. TDK is a two-dimensional, non-equilibrium nozzle performance code.[7] The TDK code evaluates the hot-gas side heat flux with T_{GW} predictions from RTE. The code options which were used for this study were One-Dimensional Equilibrium (ODE), Two-Dimensional Equilibrium (TDE), and Boundary-Layer Module (BLM). ODE and TDE assume chemical equilibrium composition at ideal rocket chamber conditions. Ideal rocket chamber combustion results in the hottest combustion gas temperature, since perfect combustion is assumed and no losses are accounted for. Using the hottest combustion chamber environment allowed for a more conservative approach to the study. ODE takes an assigned enthalpy and pressure and uses the free-energy minimization method to compute the equilibrium conditions. TDE uses the method of characteristics assuming that the process is in a state of shifting chemical equilibrium. BLM was used to introduce the effects of a boundary layer on the hot-gas-side heat transfer. BLM accounts for losses

in performance due to compressible laminar and turbulent wall boundary layers. A two-point finite difference method, developed by Keller and Cebeci, is employed to calculate the boundary layer properties and the turbulent boundary layer is modeled by the Cebeci-Smith eddy-viscosity formulation.[18,19] BLM considers the effects of transverse, as well as longitudinal, curvature effects. It also includes the effects of heat transfer and drag. One limitation of TDK is that the mixture ratio input is limited to a constant value in the axial direction.

4.4.3 RTE and TDK Coupled

RTE and TDK were coupled by iterating between heat transfer rate and T_{GW} in order to obtain the hot-gas side heat transfer. The process begins with running RTE by using an assumption of C_G for equation (2), based upon empirical combustion chamber data. The T_{GW} values predicted by RTE are input into TDK. TDK is run to obtain the predicted heat flux. The heat flux from TDK is input back into the RTE code, and the process is started over. However, for this second iteration, the hot-gas-side heat transfer coefficient and heat flux calculations are bypassed. These calculations are replaced by the heat flux values from TDK.

The RTE with TDK method of predicting the T_{GW} and coolant pressure drop has been compared against experimental results obtained during HARCC validation tests.[2] The method was able to predict experimental coolant rib thermocouple temperatures within an average of 9 percent and experimental coolant pressure drops within an average of 25 percent.

For HARCC, considering T_{GW}, RTE with TDK is limited by the assumption of a uniform coolant temperature in the coolant channels, at a given cross-section. Previous analysis has shown that HARCC could produce thermally stratified flow in the tall coolant channels, if there is significantly reduced secondary flow mixing.[20] Subse-

quently, several experimental and analytical studies have been conducted to investigate the secondary flow effects related to HARCC, and obtain results on the mixing of the coolant flow.[21,22,23,24] These results indicate that secondary flow vorticies do occur, and the thermal stratification may not be as severe. Modeling of the flow and coolant temperature in RTE with TDK would require significant restructuring of the code. As stated above, the use of RTE with TDK to predict T_{GW} has been shown to predict past experimental results well.[2] Therefore, for this analysis, the use of a uniform coolant temperature at a given cross-sectional area was acceptable.

The coolant pressure drop predictions, from RTE with TDK, were consistently lower when compared with experimental coolant pressure drops.[2] One reason for this discrepancy is the RTE code was run assuming smooth channels. However, the actual combustion chamber channels did not have perfectly smooth channels in the bifurcation regions, and possible burrs existed in the coolant entry and exit manifolds, after welding. Each of these were localized to particular channels or non-uniform in a circumferential region of the chamber. These manufacturing consequences could account for the discrepancy in the code predictions and data, and are very difficult to predict and model due to the non-uniformity. Also, as stated in section 4.4.1, RTE coolant pressure drop predictions do not account for sudden changes in coolant flow area. This consequence could also account for the discrepancy in the code predictions, since the combustion chamber tested had sudden area changes from the use of bifurcated cooling channels. For this study, smooth coolant channels were assumed in order to make a comparison between each coolant channel design. Although the assumption of smooth coolant channels would not give the most accurate assessment of coolant pressure drop, it would eliminate error for assumptions in localized manufacturing consequences.

4.5 Coolant Channel Design Method

The coolant channel design method used RTE and TDK coupled to evaluate T_{GW} and coolant pressure drop. Using the T_{GW} and coolant pressure drop, a coolant channel design was formulated which would reduce the T_{GW} in the hot throat region from the baseline. Figure 6 shows a schematic of a conventionally cooled T_{GW} profile and a desired T_{GW} profile using HARCC. A reduction of the T_{GW} in the throat region from 778 K (1400 °R) to below 667 K (1200 °R) was used as the desired HARCC profile. The T_{GW} limit of 667 K (1200 °R) was chosen based upon an experimental study of the fatigue life of OFE copper thrust chambers.[25] This study showed that a reduction of the T_{GW} from 778 K (1400 °R) to 667 K (1200 °R) could more than double the number of thermal cycles before failure.
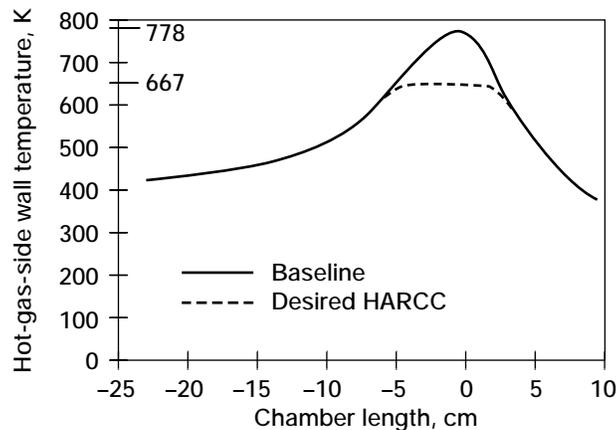
Figure 6.—Schematic of desired hot-gas-side wall temperature using high aspect ratio cooling.

The flow chart given in Figure 7 represents the method used to develop the coolant channel designs to obtain T_{GW} profiles for each design which would most closely match the desired HARCC profile shown in Figure 6. The axial locations evaluated along the combustion chamber contour are indicated in Figure 4. As shown in Figure 7,
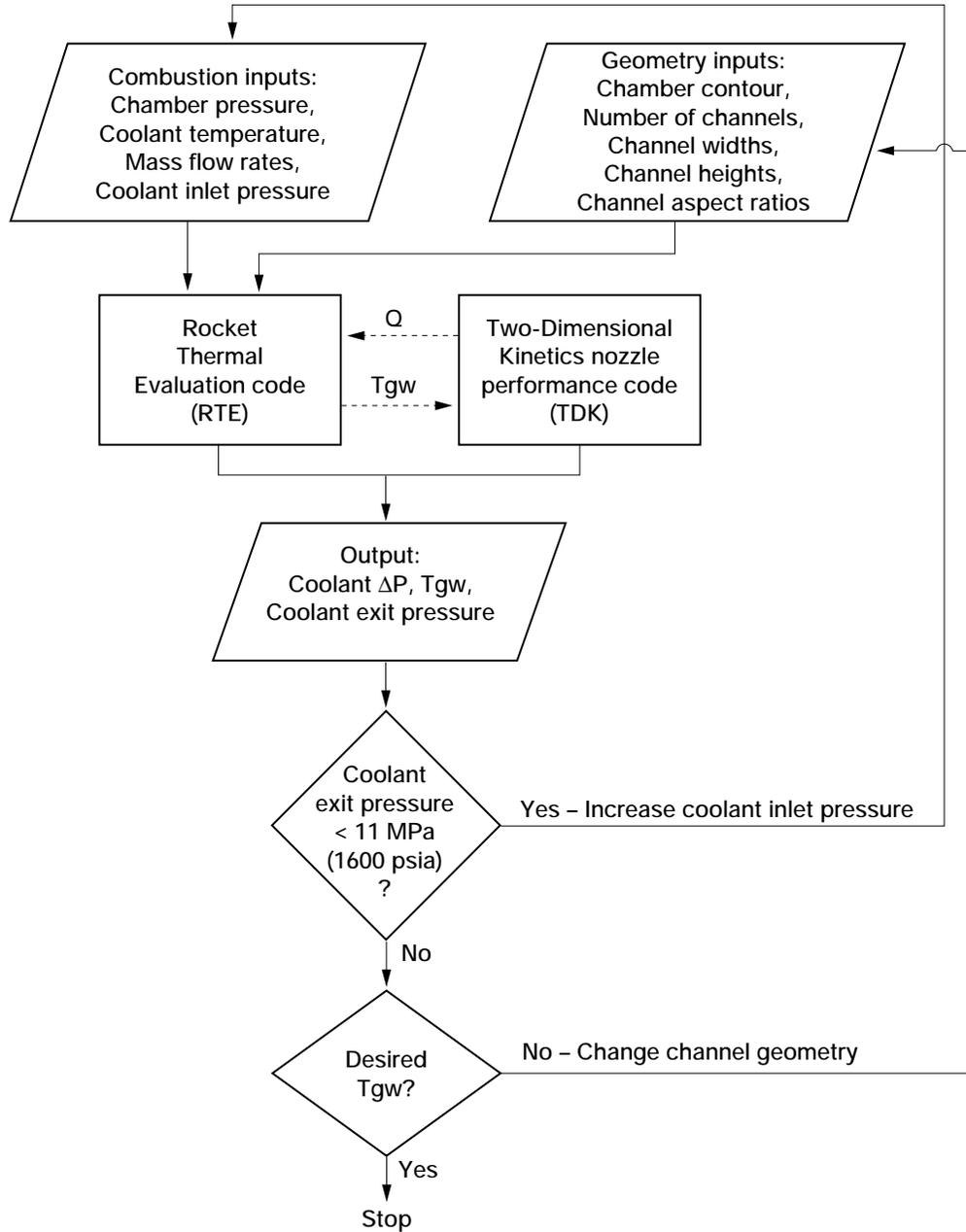
Figure 7.—Flow chart of computer design and analysis method.

the coolant inlet pressure was increased until the coolant exit pressure was above the chamber pressure. This was done to simulate the positive pressure differential needed during actual combustion in order to prevent back flow into the coolant channels in the case of a failure. Once the coolant pressure was corrected, the coolant channel geometry was modified based upon the resultant T_{GW}. In order to modify the coolant channel geometry, and maintain the same total coolant channel flow area as the baseline, the coolant channel width was varied. Without considering fabrication, the resultant coolant channel height, aspect ratio, and landwidth (coolant channel rib thickness) was accepted. When fabrication was taken into consideration, the coolant channel width was again varied, but the coolant channel height, aspect ratio, and landwidth were monitored to comply with the fabrication criteria described below.

4.6 Fabrication Criteria

When fabrication was taken into consideration, it was limited to current milling capabilities. The most important of these are:

- Aspect ratios ≤ 8
- Coolant channel heights ≤ 0.51 cm (0.20 inches)
- Coolant channel widths ≥ 0.051 cm (0.02 inches)
- Coolant channel landwidths ≥ 0.051 cm (0.02 inches)
- No sharp changes in coolant channel width or height (except the width changes for the stepped channel design)

The bifurcated channels had an additional fabrication consideration. With current milling techniques, it is very difficult to perfectly bifurcate a channel. Usually there is a transition section created during milling. This transition is depicted in Figure 8. The result is an exaggerated increase in flow area of the single coolant chan-
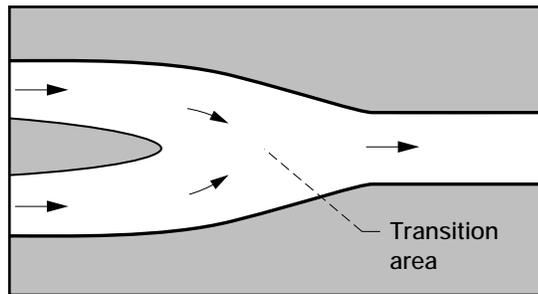
Figure 8.—Schematic of bifurcation fabrication.

nel, which reduces the heat transfer capabilities at that point, and can lead to a local increase in T_{GW}. This transition was taken into account for the bifurcated channel design. The total coolant flow area for each axial location at these bifurcation transition points was greater than the baseline design. This allowed for a more accurate assessment of the effect the transition area had on the T_{GW} for the bifurcation design.

5. Results and Discussion

Using the design and analysis methodology described, the final coolant channel designs, corresponding T_{GW}s and coolant channel pressure drops were determined and compared. Each design given in Table I was evaluated with and without consideration for fabrication. Finally, an overall design was selected and optimized. The optimized design was evaluated for effects of reduced coolant mass flow rates on T_{GW} and coolant pressure drop.

5.1 Coolant Channel Designs Without Consideration for Fabrication

The coolant channel designs were first determined without consideration for fabrication. T_{GW}s and coolant channel pressure drops were determined with the resultant geometries. The specific coolant channel geometries are given in Tables A-I through A-VII, in Appendix A, for each of the designs without consideration for fabrication.

Each design attempted to reproduce the desired HARCC T_{GW} profile given in Figure 6. Figures 9 through 15 show each design's actual T_{GW} compared with the baseline T_{GW}. As shown in Figures 9 through 15, each design resulted in T_{GW}s below the limit of 667 K (1200 °R), with a temperature profile similar to the profile given in Figure 6. Table II shows the highest T_{GW} and the coolant pressure drop for each of the designs, without considering fabrication. As shown in Table II, T_{GW} reductions from 16.5 percent to 22 percent were obtained. Figures 10, 12, and 15, which correspond to designs 2, 4, and 7, show the entire T_{GW} profiles well below the baseline due to the use of 200 cooling channels throughout the entire chamber region. Figures 14 and 15, which correspond to designs 6 and 7, do not have a smooth reduced T_{GW}, but rather show fluctuations in the temperature profile. This is due to the abrupt changes in the coolant channel width based upon the stepped coolant channel design configuration.

Table II.—Comparison of Maximum Predicted Hot-Gas-Wall Temperatures and
Total Coolant Channel Pressure Drops

Design No.	Without Consideration for Fabrication		Considering Fabrication	
	T_{GW} K (°R)	ΔP MPa (psi)	T_{GW} K (°R)	ΔP MPa (psi)
Baseline	764 (1376)	3.7 (540)	764 (1376)	3.7 (540)
1	639 (1150)	4.7 (675)	700 (1260)	4.2 (610)
2	600 (1080)	5.0 (730)	608 (1094)	5.0 (730)
3	637 (1147)	4.5 (650)	702 (1263)	4.0 (575)
4	611 (1099)	4.6 (670)	609 (1096)	4.8 (690)
5	618 (1113)	4.0 (580)	613 (1103)	4.1 (590)
6	636 (1144)	4.4 (640)	703 (1265)	3.9 (560)
7	602 (1083)	4.7 (680)	610 (1098)	4.7 (675)

Coolant channel pressure drops were also calculated for each design. Each of the designs resulted in a higher coolant pressure drop than the baseline. These pressure drop increases ranged from 7.5 percent to 33 percent. As expected, the highest coolant pressure drop came from design 2. This was due to using high aspect ratio cooling throughout the entire chamber, and using 200 cooling channels for the entire length of the chamber. The lowest coolant pressure drop increase (7.5 percent), came from design 5, which used bifurcated coolant channels.

All of the designs were able to produce T_{GW} profiles similar to the profile shown in Figure 6. Table III shows the significant geometry requirements to obtain the reduced T_{GW}s shown in Figures 9 through 15. As shown in Table III, designs 1, 3, and 6 have extremely high aspect ratio requirements of 40, channel heights up to 1.02 cm (0.400 in), and channel widths of 0.025 cm (0.010 in). Designs 2, 4, 5, and 7 have geometry requirements that are not as extreme as designs 1, 3, and 6, and are closer to fabrication capabilities.

Table III.—Geometry Comparisons of Designs Without Consideration for Fabrication

Design No.	Highest Aspect Ratio	Maximum Channel Height cm (in.)	Minimum Channel Width cm (in.)	Minimum Landwidth cm (in.)
1	40.0	1.02 (0.400)	0.025 (0.010)	0.183 (0.072)
2	6.2	0.318 (0.125)	0.046 (0.018)	0.056 (0.022)
3	40.0	1.02 (0.400)	0.025 (0.010)	0.165 (0.065)
4	5.0	0.254 (0.100)	0.051 (0.020)	0.043 (0.017)
5	8.9	0.587 (0.231)	0.051 (0.020)	0.043 (0.017)
6	40.0	1.02 (0.400)	0.025 (0.010)	0.135 (0.053)
7	6.2	0.292 (0.115)	0.046 (0.018)	0.043 (0.017)

Once the coolant channel designs were determined, the seven designs were compared. The use of HARCC throughout the entire chamber length, designs 1 and 2, produced T_{GW} profiles similar to the other designs. However, the coolant pressure drop increases incurred were 24 and 33 percent, respectively. The use of 200 channels throughout the entire chamber, designs 2, 4, and 7, produced the highest benefit to the T_{GW} with reductions of 20 to 22 percent, but incurred coolant pressure drop increases of 22 to 33 percent. All of the HARCC designs produced a reduction in T_{GW} of at least 16.5 percent, with coolant channel pressure drop increases as low as 7.5 percent. Based upon the T_{GW} and coolant channel pressure drop, design 5 resulted in the highest overall benefit. Although design 5 does not have the 22 percent reduction in T_{GW} as design 2, it does have a 19 percent T_{GW} reduction and the lowest coolant pressure drop increase of 7.5 percent.

Figure 9.—Hot-gas-side wall temperature comparison of Design 1 and baseline, without consideration for fabrication.
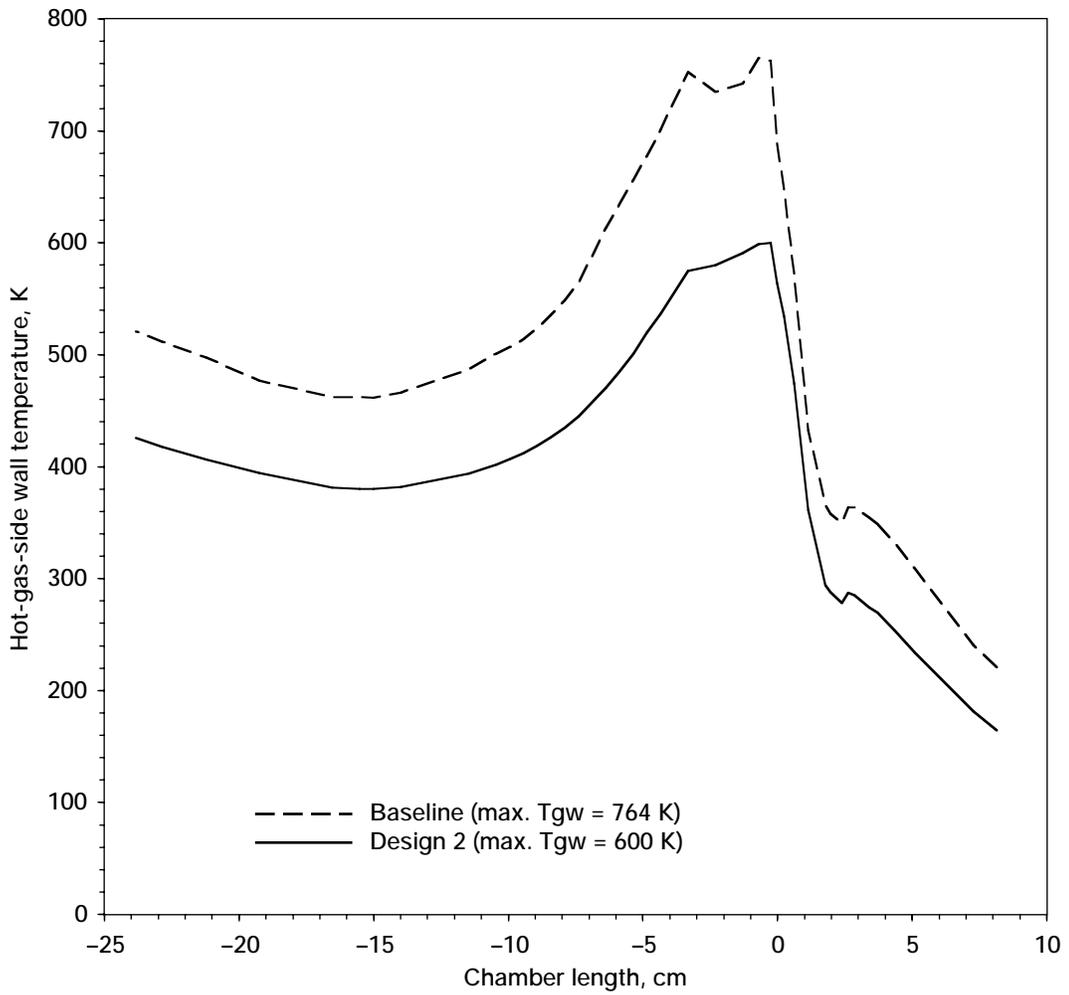
Figure 10.—Hot-gas-side wall temperature comparison of Design 2 and baseline, without consideration for fabrication.
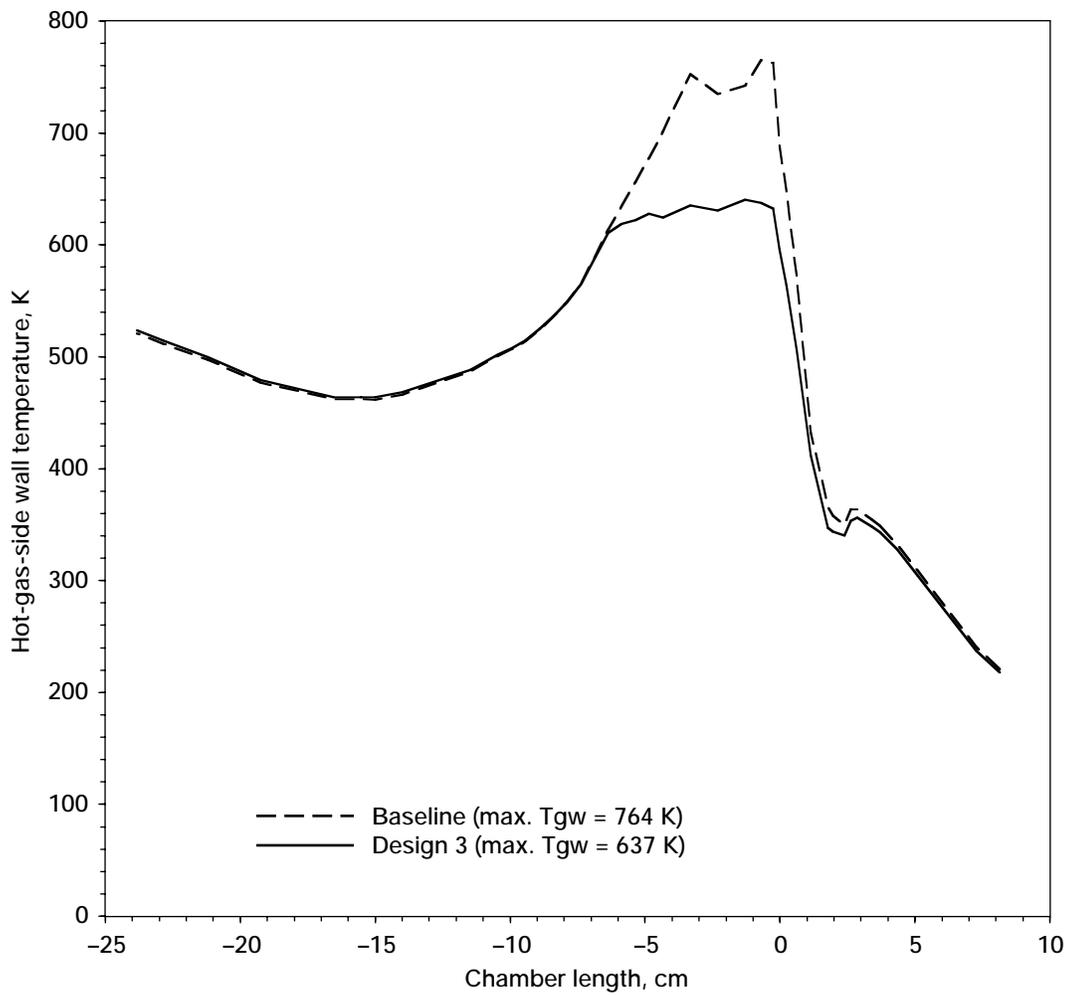
Figure 11.—Hot-gas-side wall temperature comparison of Design 3 and baseline, without consideration for fabrication.
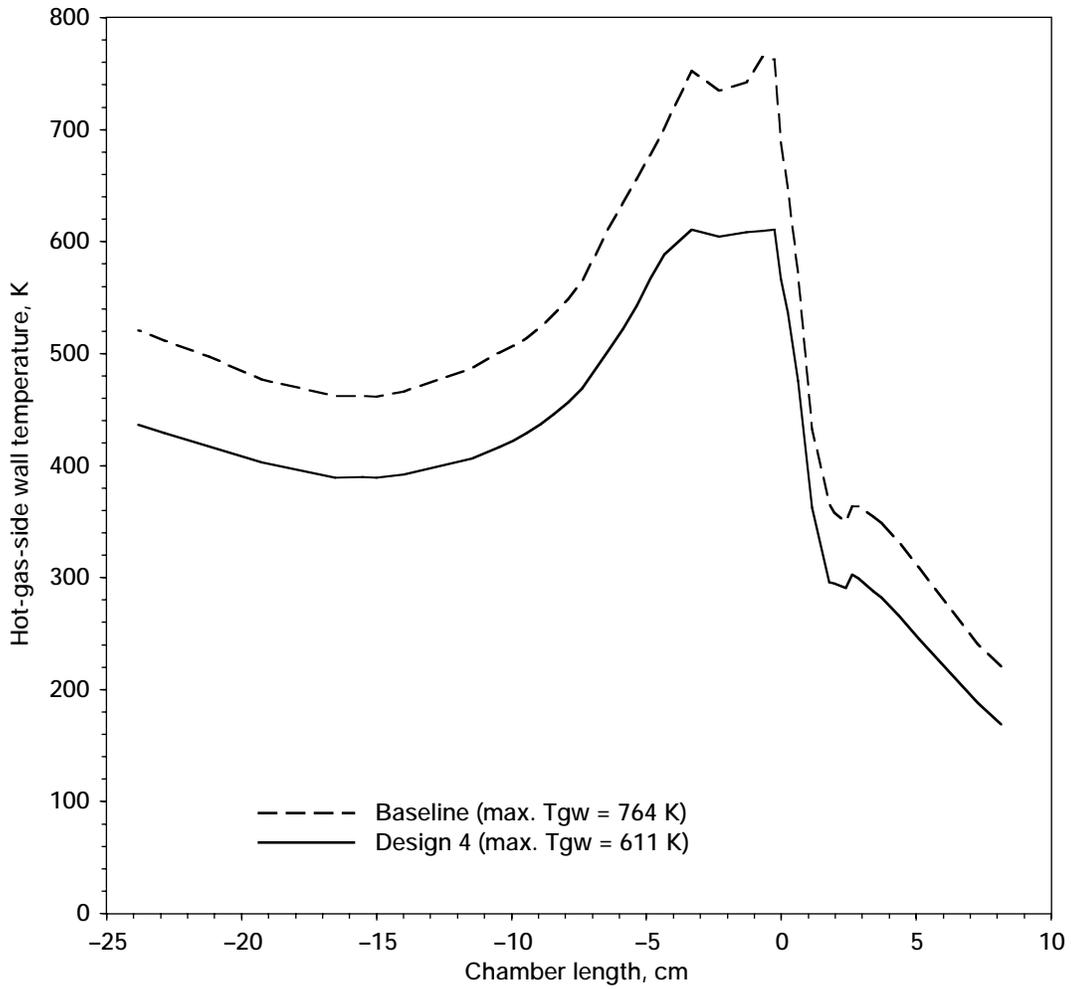
Figure 12.—Hot-gas-side wall temperature comparison of Design 4 and baseline, without consideration for fabrication.
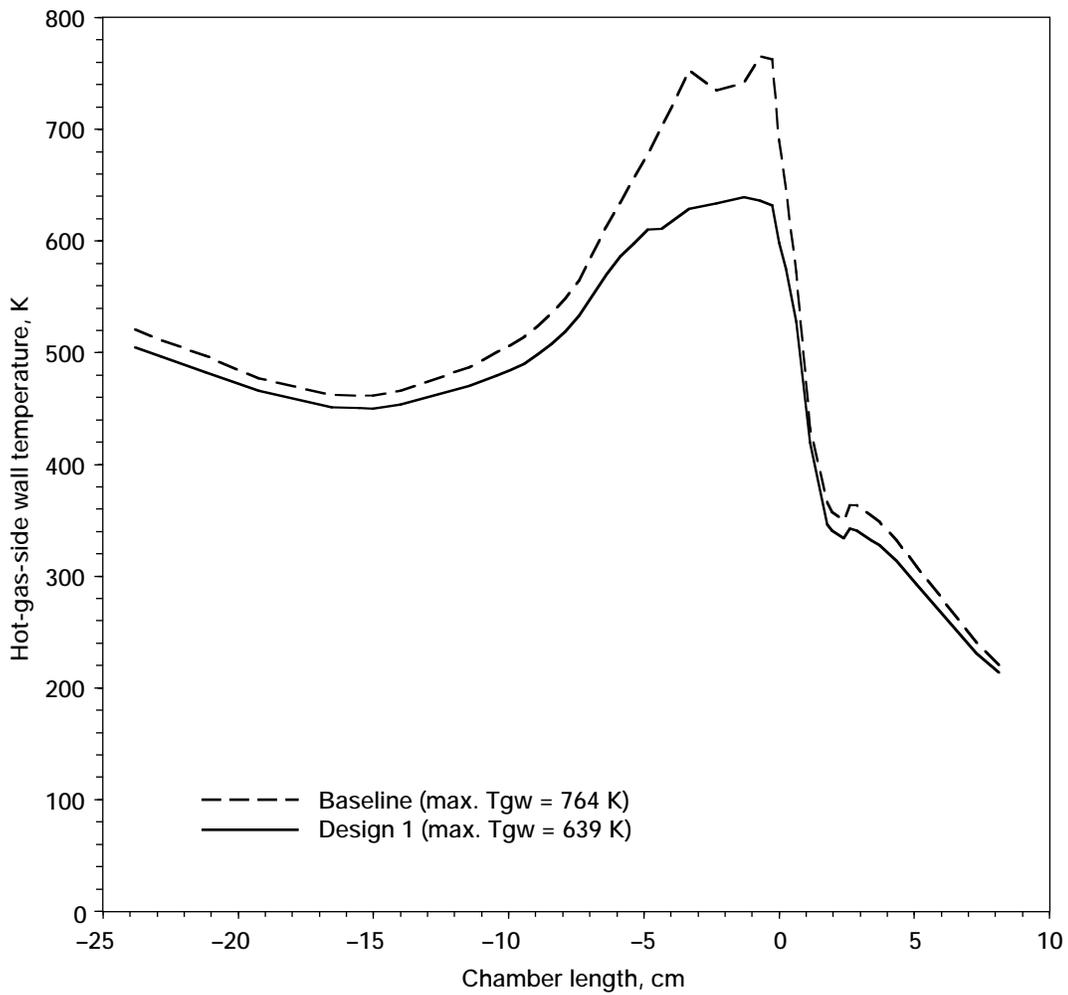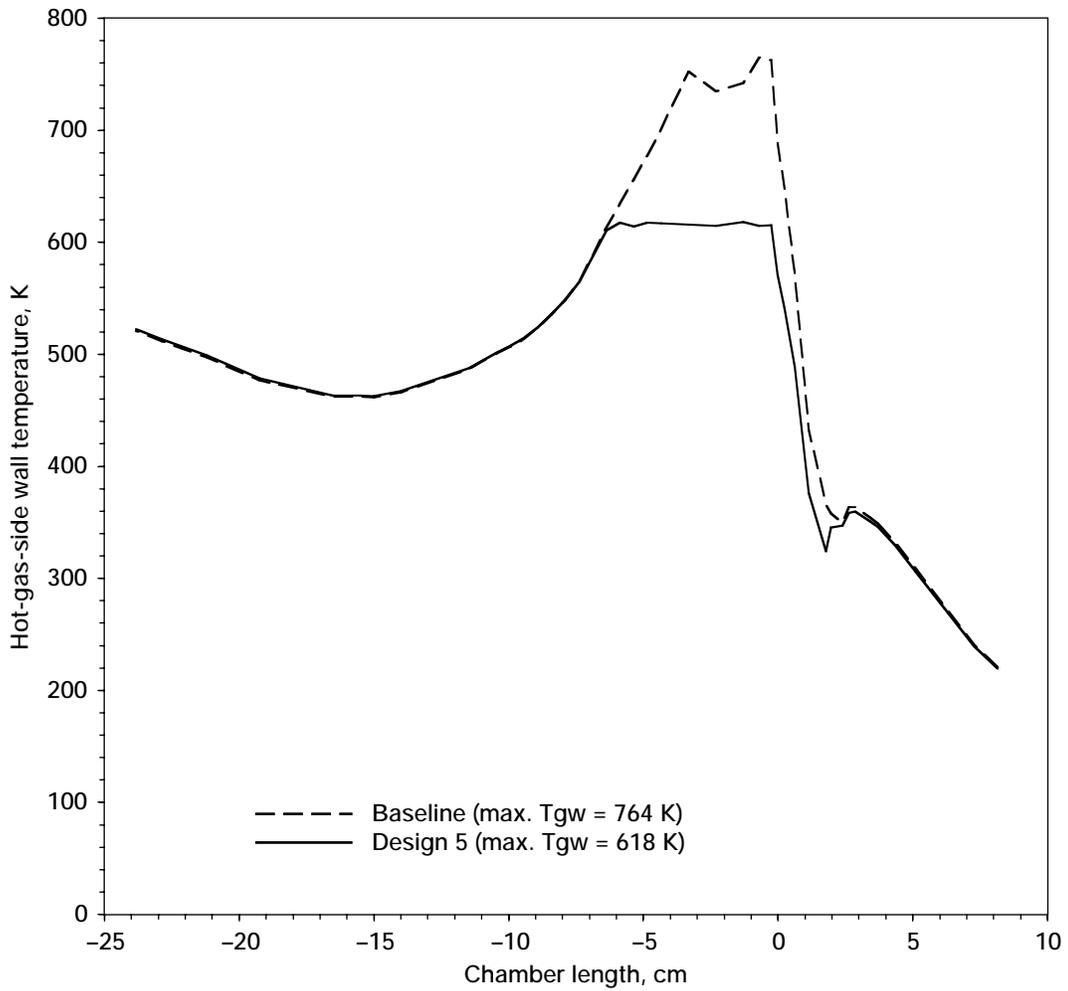
Figure 13.—Hot-gas-side wall temperature comparison of Design 5 and baseline, without consideration for fabrication.
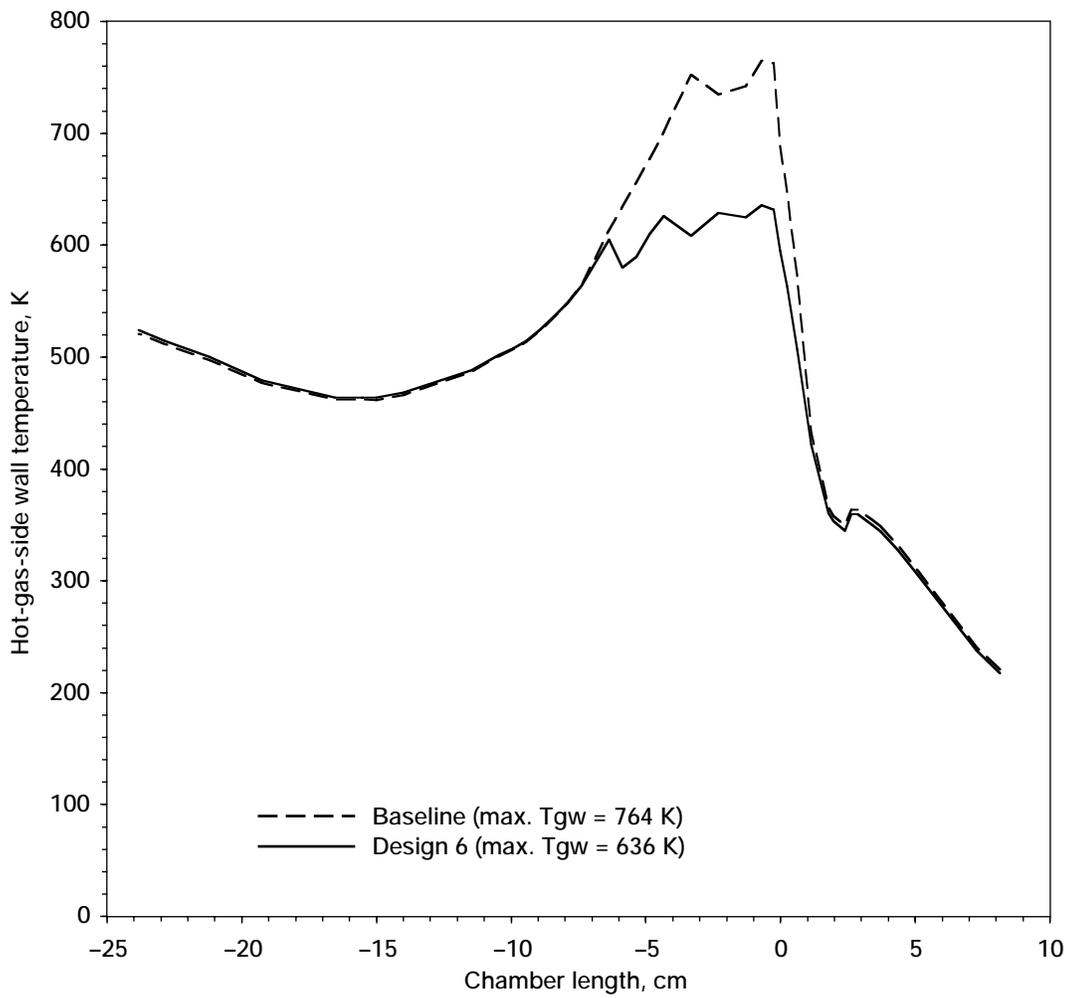
Figure 14.—Hot-gas-side wall temperature comparison of Design 6 and baseline, without consideration for fabrication.
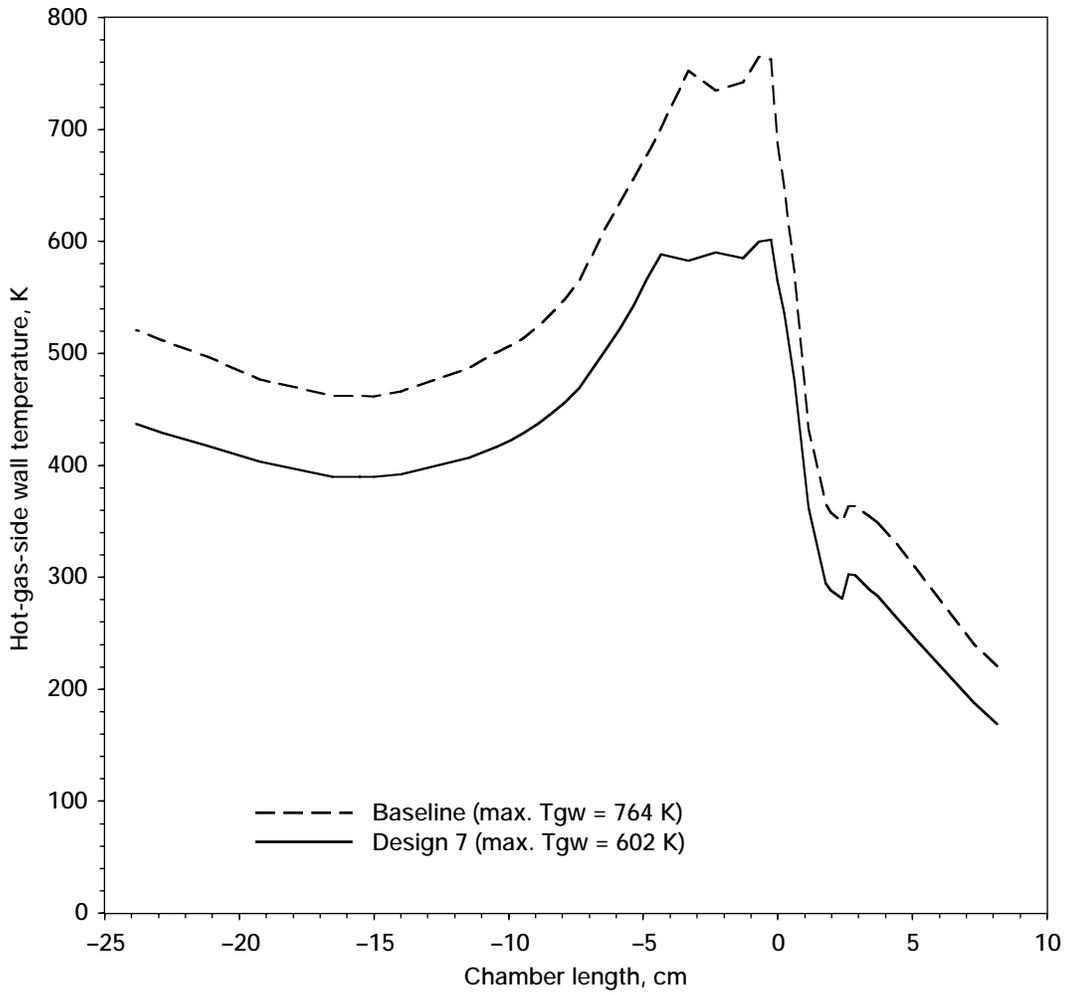
Figure 15.—Hot-gas-side wall temperature comparison of Design 7 and baseline, without consideration for fabrication.

5.2 Coolant Channel Designs Considering Fabrication

After the coolant channel designs had been determined to achieve the T_{GW} profile shown in Figure 6, the designs were modified for fabrication. T_{GW}s and coolant channel pressure drops for each design were then determined. The specific coolant channel geometries are given in Tables A-VIII through A-XIV, in Appendix A, for each of the designs considering fabrication.

Each design was evaluated to obtain its T_{GW} profile based upon fabrication constraints. Figures 16 through 22 show each design's T_{GW} compared with the baseline T_{GW} and the T_{GW} achieved without considering fabrication. Figures 16, 18, and 21, which correspond to designs 1, 3, and 6, show T_{GW} profiles with only modest decreases in temperature once fabrication was taken into consideration. Table II shows the highest T_{GW} and coolant pressure drop for each of the designs after considering fabrication. As shown in Table II, designs 1, 3, and 6 have temperature reductions of 8 percent. Figures 17, 19, and 22, which correspond to designs 2, 4, and 7, show minimal change in the T_{GW}s once fabrication was considered. These designs retained the 20 percent reduction in T_{GW}, as shown in Table II. Design 5 resulted in the most dramatic change in T_{GW} profile (see Figure 20) once fabrication was considered. As expected, sharp temperature increases in the bifurcation transition areas did occur. However, the area of 200 channels was extended well into the combustion chamber to place the bifurcation point beyond the critical heat transfer area and reduce the temperature peaks. This resulted in some over cooling of the chamber upstream of the throat.

Coolant channel pressure drops were calculated for each design. Each of the designs resulted in a higher coolant pressure drop than the baseline. These pressure drop increases ranged from 2 percent to 33 percent. Again, the highest coolant pressure drop came from design 2. The lowest coolant pressure drop increase (2 percent), came

from design 6, which used 100 stepped coolant channels. The coolant pressure drops were lower, once fabrication was considered, for designs 1, 3, and 6, due to limiting the coolant channel height to 0.51 cm (0.20 in) for fabrication.

Imposing fabrication constraints on the seven designs impacted the coolant channel geometries as well as the T_{GW} and coolant pressure drops. However, it was still possible to meet the desired T_{GW} with an acceptable coolant pressure drop. The fabrication constraints greatly modified designs 1, 3, and 6. This was due to the reduction in their highest aspect ratio from 40 down to the limit of 8. This raised the maximum T_{GW} for designs 1, 3, and 6 to above the limit of 667 K (1200 °R) (see Table 3). However, lowering the aspect ratio of these designs greatly reduced their coolant pressure drops. Designs 2, 4, and 7 did not have a significant change once fabrication was considered, since their geometries were close to the fabrication constraints initially (see Table II). The T_{GW} profiles for designs 2, 4, and 7 did vary with consideration for fabrication, but did not go above the limit of 667 K (1200 °R). Likewise, the coolant pressure drops for these designs did not vary greatly. Design 5 did have significant geometry changes with consideration for fabrication, although it was already close to the fabrication limits. This was due to the inclusion of the transition area in the bifurcation regions and the need to eliminate the T_{GW} spikes in these regions. Although design 5's geometry made a dramatic change, the maximum T_{GW} was below the 667 K (1200 °R) limit, and the coolant pressure drop remained about the same. The fabrication constraints imposed did limit some of the designs in meeting the T_{GW} desired, however, a design was possible which was able to reduce the T_{GW} below the 667 K (1200 °R) limit without a severe coolant pressure drop penalty.

Once fabrication was taken into consideration, the seven designs were compared again. As in the case without consideration for fabrication, the use of HARCC

throughout the entire chamber length, designs 1 and 2, produced similar T_{GW} profiles to those that used HARCC only in the throat region. Designs 1 and 2 also continued to have higher pressure drop increases, 11 and 33 percent respectively. Therefore, using HARCC throughout the entire chamber length does not have significant advantage over using HARCC in the throat region, but does have a significant adverse impact on coolant pressure drop. The use of 200 channels throughout the entire chamber length, designs 2, 4, and 7, again produced the highest benefit to the T_{GW}, after fabrication was considered, with reductions of 19.5 to 20 percent, but still incurred coolant pressure drop increases of 24 to 33 percent. This shows that using 200 channels for the entire chamber length could significantly benefit the T_{GW} profile, but would have a high coolant pressure drop penalty. All of the HARCC designs, once fabrication was accounted for, produced reductions in T_{GW} of at least 8 percent, with as little as a 2 percent increase in coolant pressure drop (design 6, in Table II). This shows that the use of HARCC benefits the T_{GW} independent of channel shape. Based upon the T_{GW} profile and coolant pressure drop, design 5 was again the design which would result in the highest overall benefit. It had a 20 percent reduction in T_{GW} and a 9 percent increase in coolant pressure drop.

Figure 16.—Hot-gas-side wall temperature comparison of Design 1 and baseline, with and without consideration for fabrication.

Figure 17.—Hot-gas-side wall temperature comparison of Design 2 and baseline, with and without consideration for fabrication.
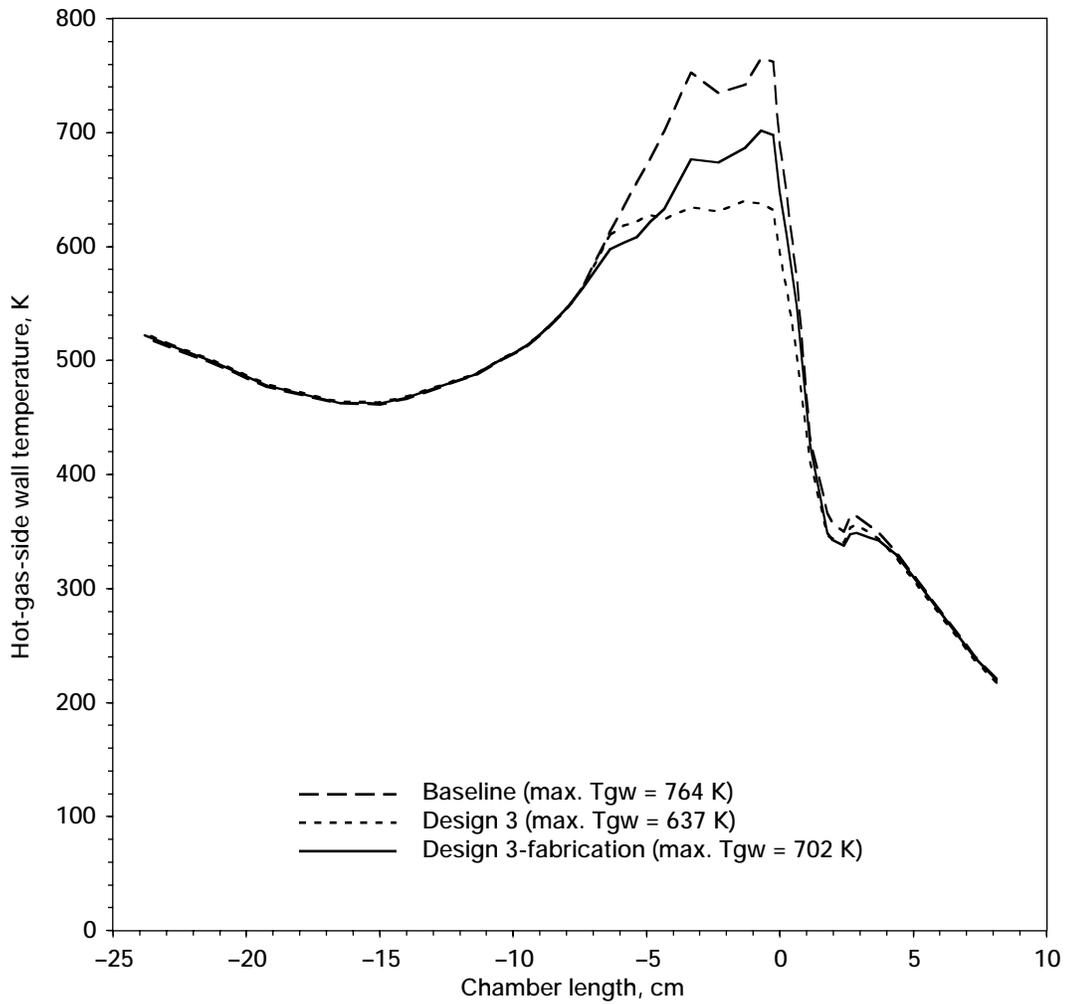
Figure 18.—Hot-gas-side wall temperature comparison of Design 3 and baseline, with and without consideration for fabrication.
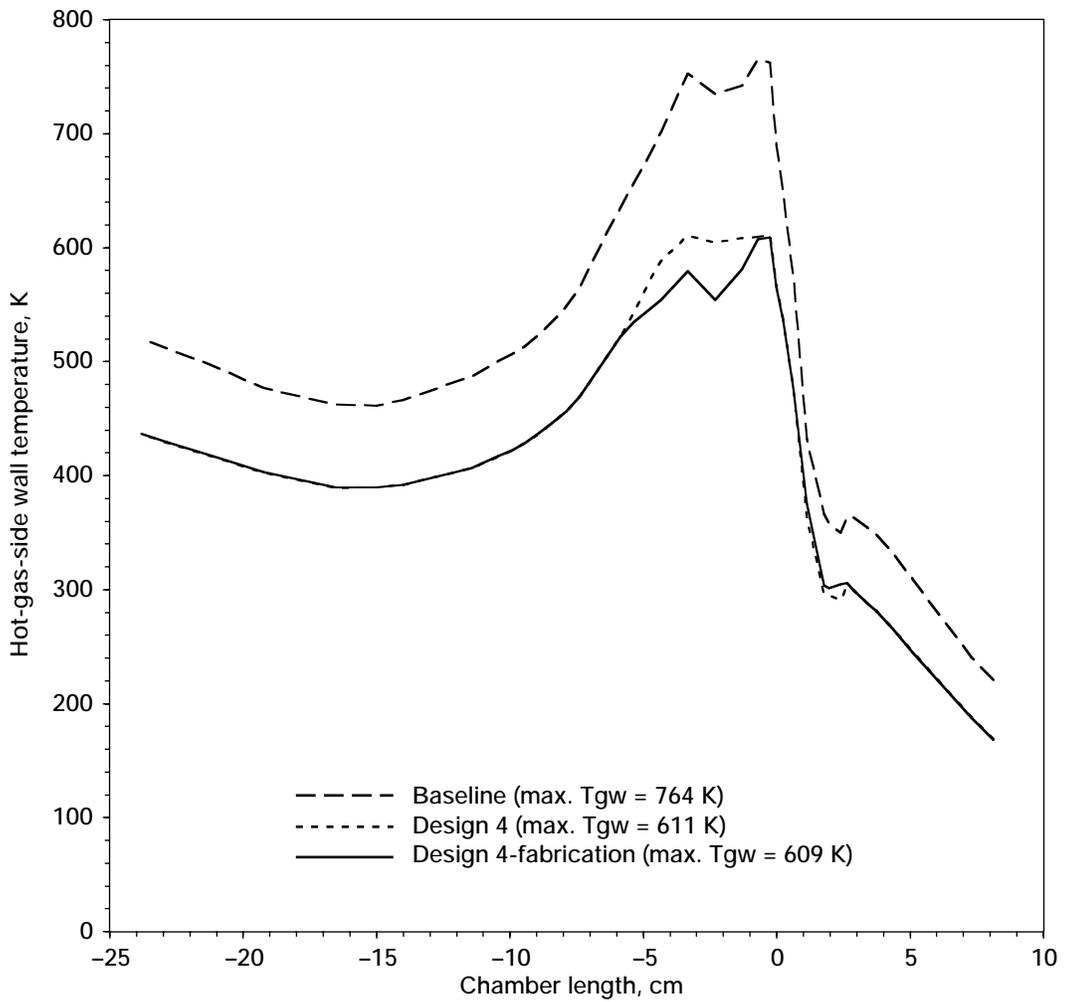
Figure 19.—Hot-gas-side wall temperature comparison of Design 4 and baseline, with and without consideration for fabrication.
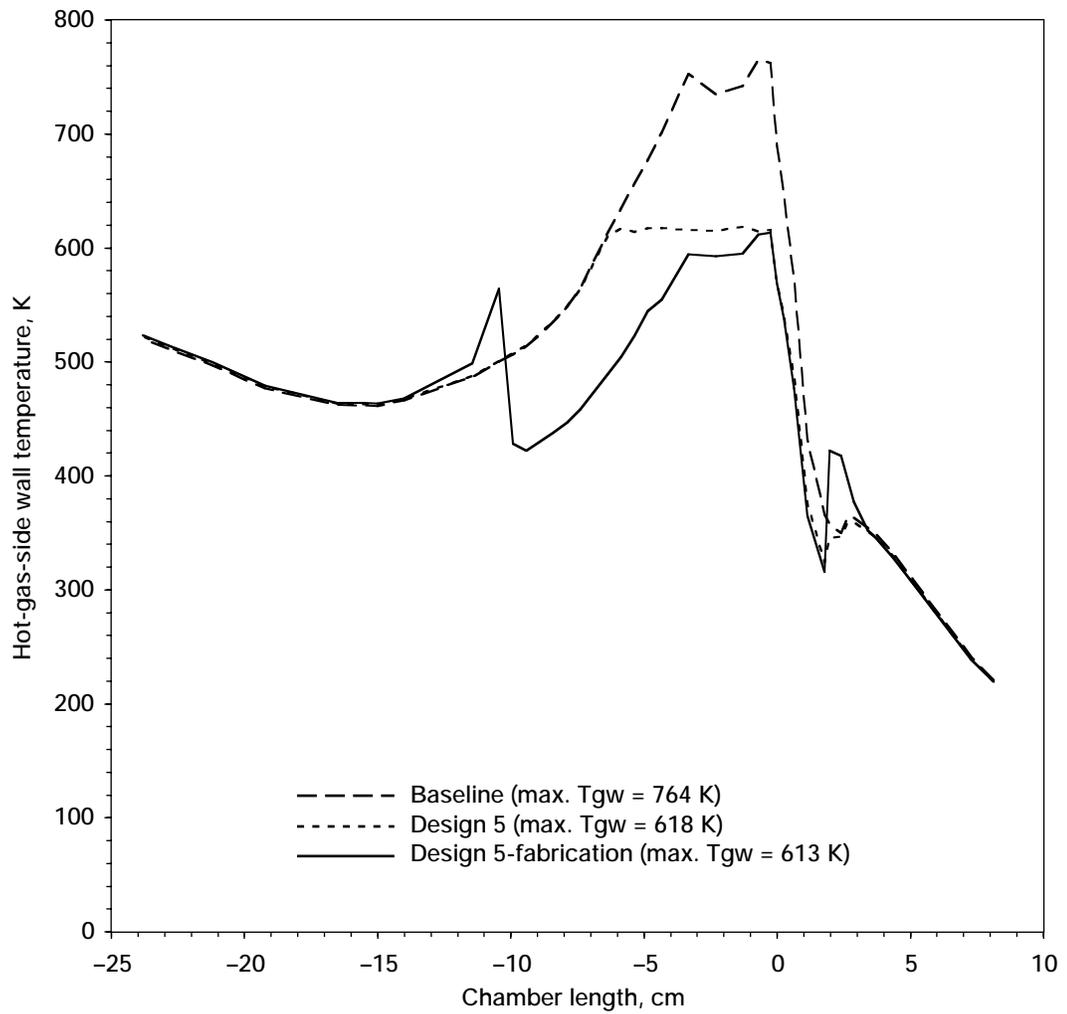
Figure 20.—Hot-gas-side wall temperature comparison of Design 5 and baseline, with and without consideration for fabrication.
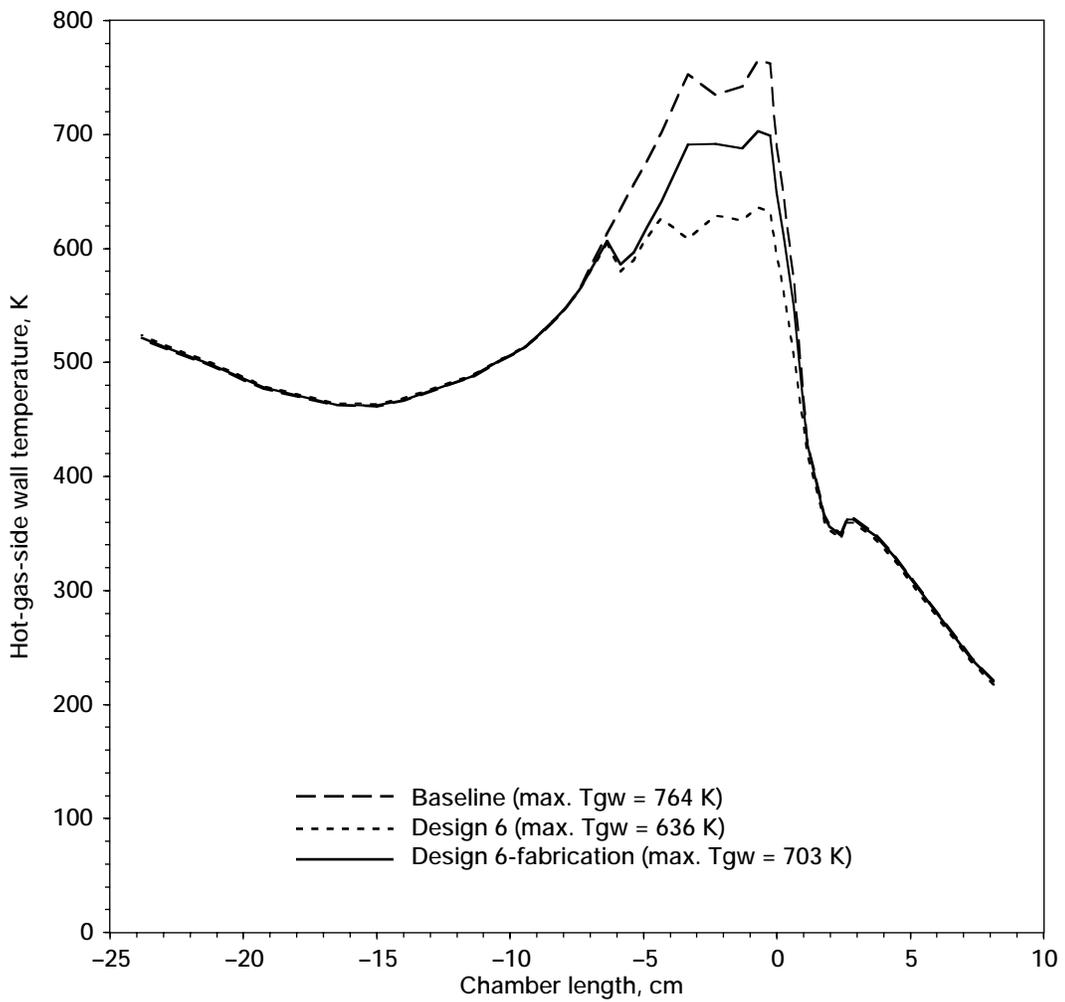
Figure 21.—Hot-gas-side wall temperature comparison of Design 6 and baseline, with and without consideration for fabrication.
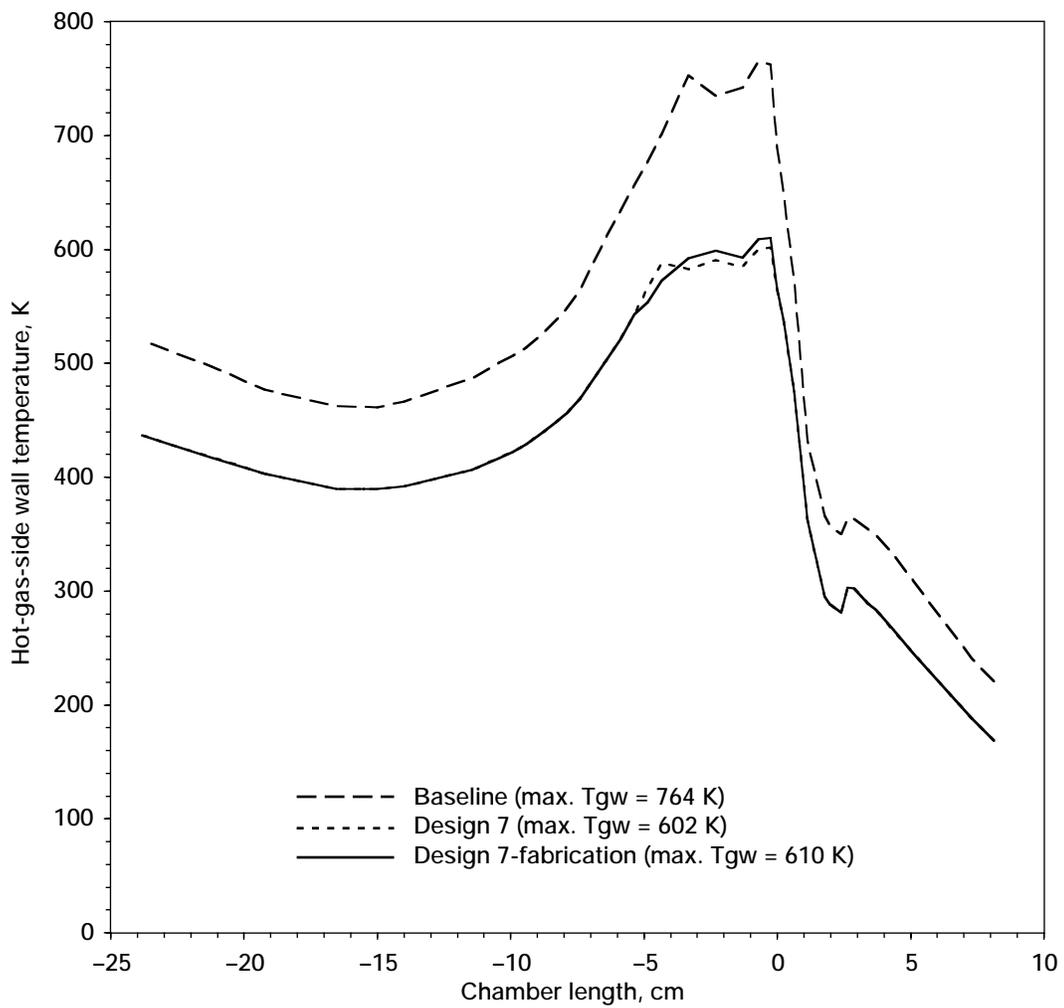
Figure 22.—Hot-gas-side wall temperature comparison of Design 7 and baseline, with and without consideration for fabrication.

5.3 Optimal HARCC Design

Once design 5 was selected to have the highest overall benefit, it was used to determine an optimal HARCC design. To determine the optimal HARCC design, the total coolant channel flow area was allowed to vary in order to obtain the desired T_{GW} profile in Figure 6, while still remaining within the constraints of the fabrication criteria. The T_{GW} profile and coolant pressure drop was then determined. The specific coolant channel geometries are given in Table A-XV, in Appendix A, for the optimal HARCC design.

The optimal HARCC design was evaluated for the T_{GW} profile. Figure 23 shows the design's T_{GW} compared with the baseline T_{GW}, the T_{GW} achieved without considering fabrication, and the T_{GW} considering fabrication. As can be seen, a T_{GW} profile similar to that shown in Figure 6 was obtained. Optimization of the coolant channel flow area allowed reductions of the T_{GW} spike in the combustion chamber area. It was also able to reduce the over cooling of the combustion chamber shown in design 5, which considered fabrication. Optimization of design 5 allowed for an 18 percent reduction in T_{GW} (maximum T_{GW} of 618 K (1113 °R)). This was only a two percent increase from design 5, which was constrained to the baseline coolant flow area.

The coolant channel pressure drop was also evaluated for the optimized design. The optimized HARCC design resulted in a coolant pressure drop of 3.5 MPa (520 psi). This is a 4 percent reduction in coolant pressure drop from the baseline configuration. All of the previous designs, which constrained the total coolant flow area to match the baseline, had increased coolant pressure drops. Therefore, by releasing the flow area constraint, the optimized HARCC design was able to significantly reduce the T_{GW} and modestly reduce the coolant pressure drop.
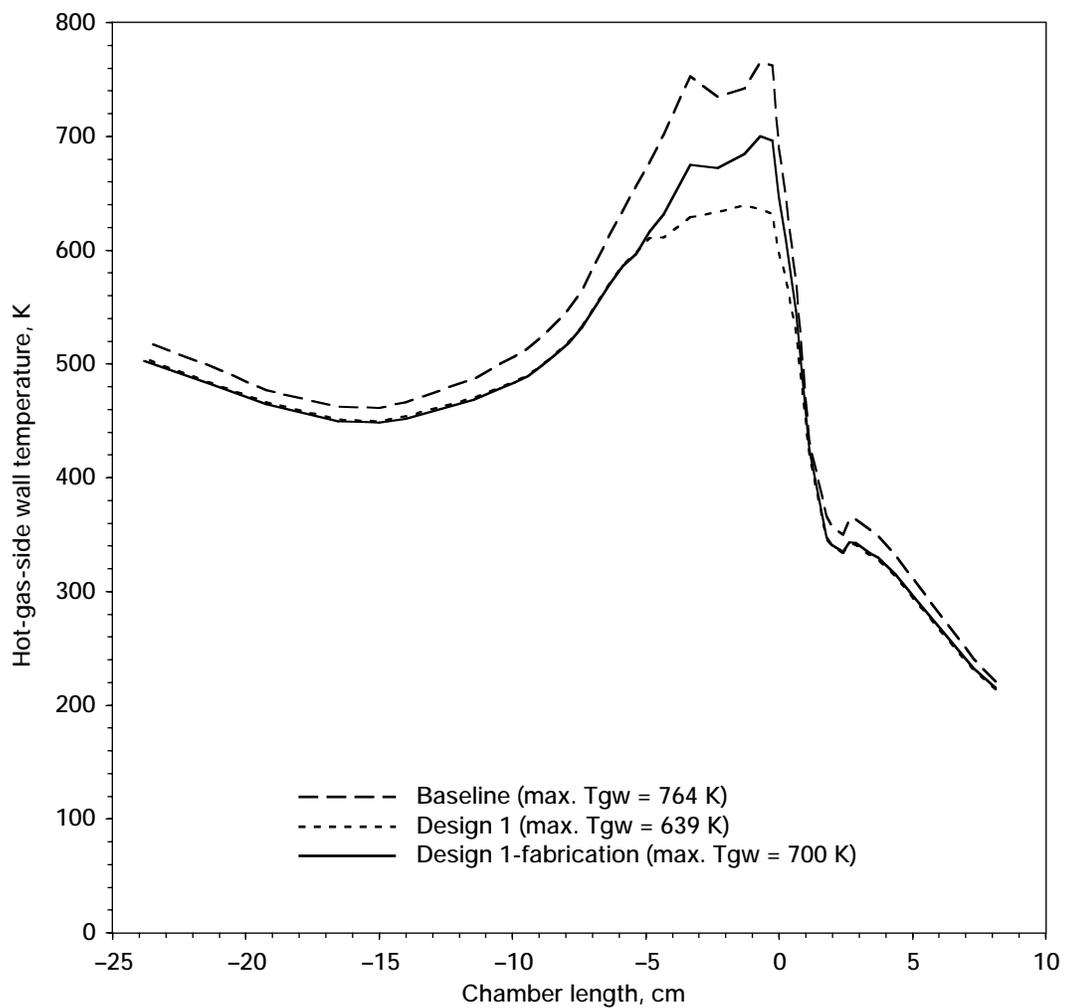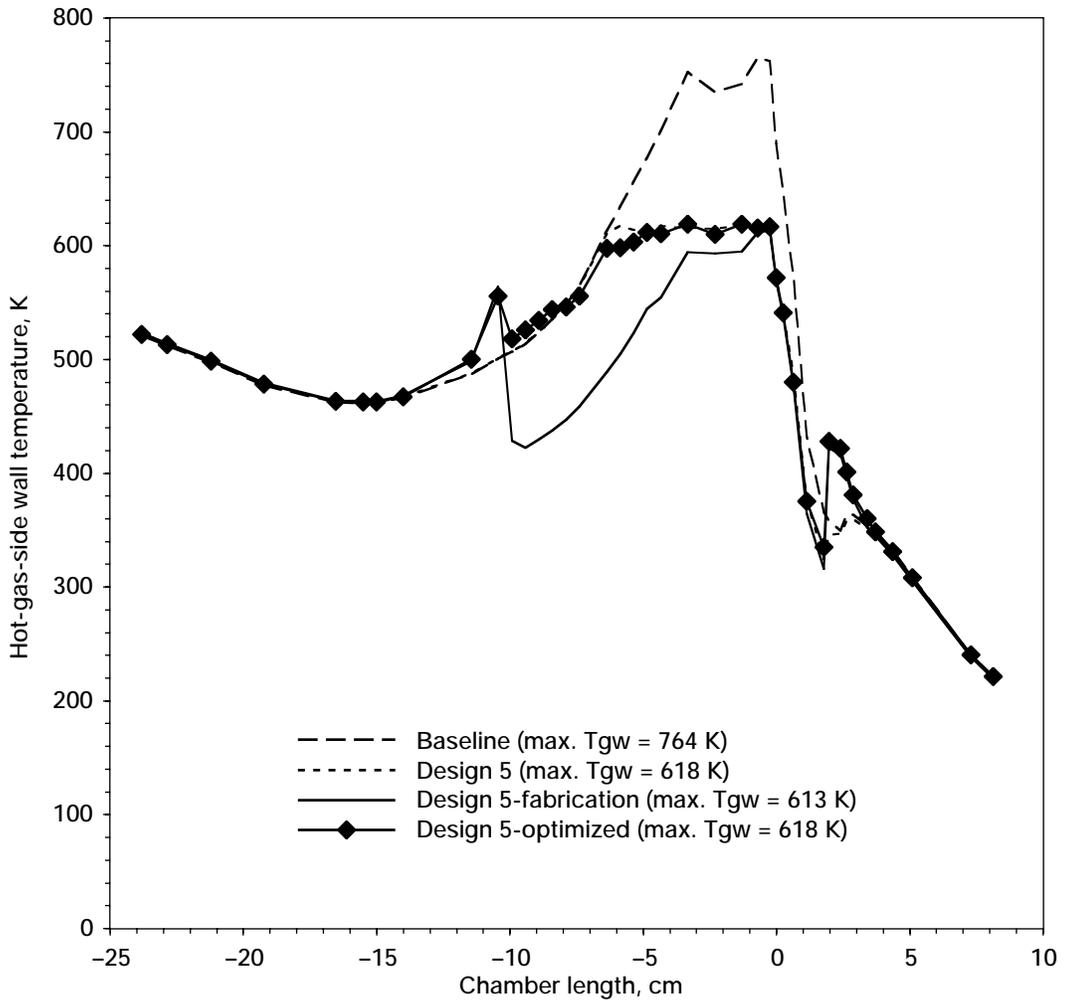
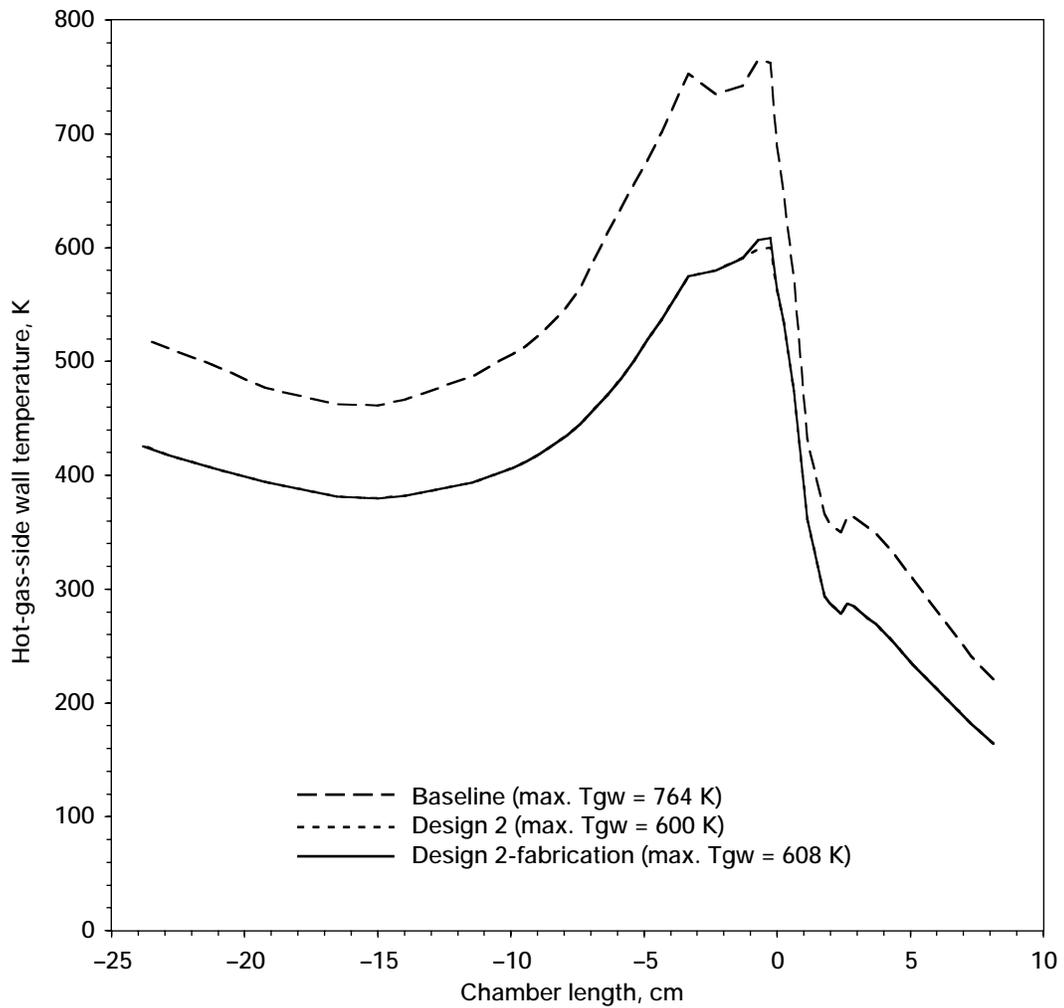Figure 23.—Hot-gas-side wall temperature comparison of Design 1 and baseline, with and without consideration for fabrication and optimized.

## 5.4 Effects of Reduced Coolant Mass Flow Rate

With the optimal HARCC design complete, the effects of reducing the coolant mass flow rate were investigated. The coolant mass flow rate for the optimal HARCC design and design 5, which considered fabrication, was reduced by ten percent increments until the T_{GW} reached approximately 778 K (1400 °R). The maximum T_{GW} values and the resultant coolant pressure drops were then evaluated and compared against the baseline maximum T_{GW} and coolant pressure drop.

The maximum T_{GW} for each of the reduced mass flow rate points was plotted against the resultant coolant pressure drops in Figure 24, along with the point for the baseline configuration. The coolant mass flow rates for both the optimal HARCC design and design 5, which considered fabrication, were reduced by 50 percent before the maximum T_{GW} reached approximately 778 K (1400 °R). Figure 24 shows, with a 40 percent reduction in coolant mass flow rate, the optimal HARCC produces T_{GW} reductions of 5 percent and coolant pressure drop reductions of 47 percent. Design 5, which considered fabrication, produced T_{GW} reductions of 8 percent and coolant pressure drop reductions of 39 percent with the same 40 percent coolant mass flow rate reduction. Although the optimal HARCC design obtains similar T_{GW}s and better coolant pressure drops than design 5, which considered fabrication, Figure 24 shows that by reducing the coolant mass flow rate for design 5, which considered fabrication, by only 10 percent, a reduction of 18 percent in T_{GW} and a reduction of 4 percent for coolant pressure drop could be realized from the baseline configuration. Therefore, if an optimal HARCC design is not possible, using HARCC with bifurcated channels can still have a benefit to both the T_{GW} and coolant pressure drop by making a minimal reduction in the coolant mass flow rate.
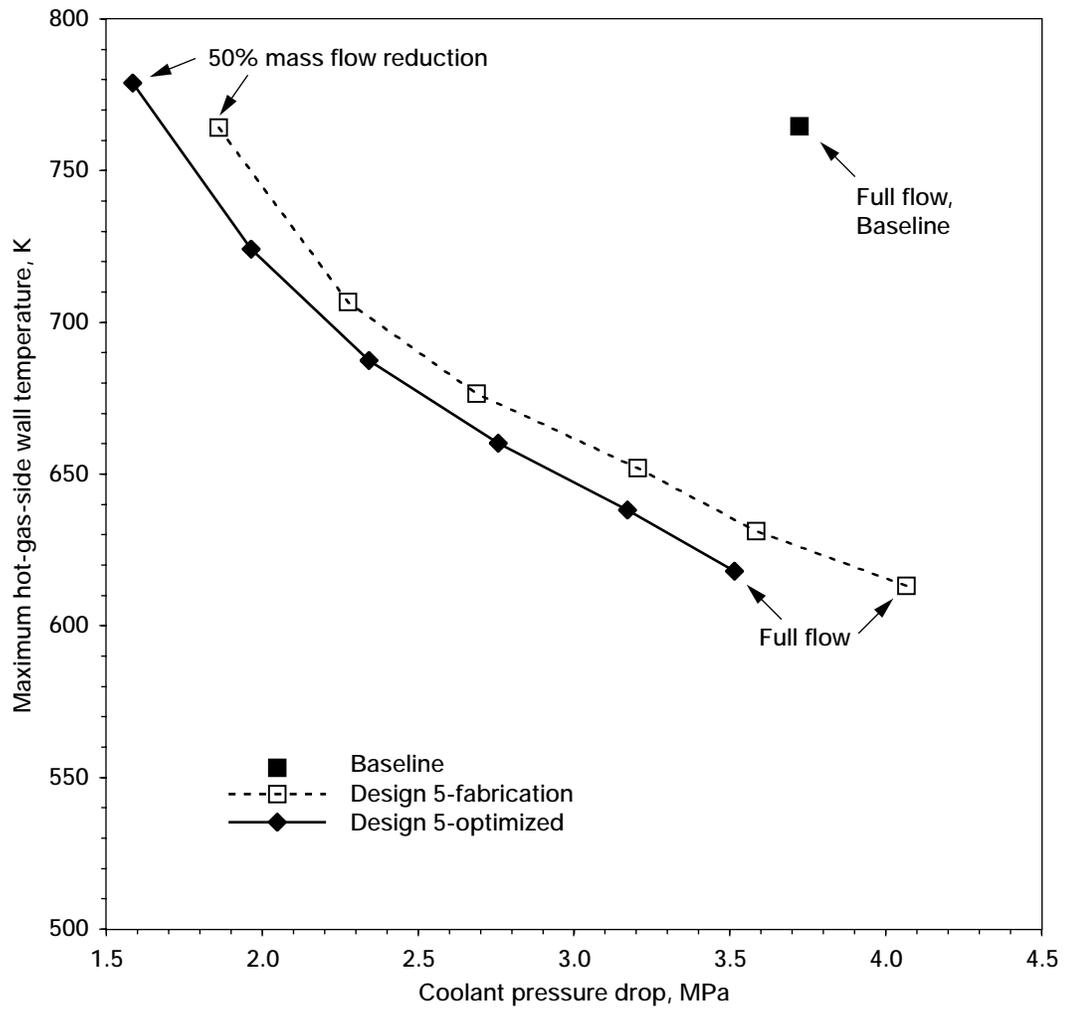
Figure 24.—Comparison of maximum hot-gas-side wall temperatures with coolant pressure drop for Design 5 and baseline, considering fabrication and optimized.

Bifurcated coolant channels have always been used for the experimental investigations of HARCC at NASA Lewis Research Center.[1,2] This was based on the enhanced fin effect of having multiple, thin ribs in the bifurcated region to enhance cooling. It was assumed that the coolant pressure drop took a penalty for the increased number of channels, but that the enhanced cooling outweighed the penalty. This study shows that the use of bifurcated high aspect ratio coolant channels enhances the cooling due to the increased number of coolant channels in the bifurcated region, but does not greatly increase the coolant pressure drop over a chamber without bifurcated coolant channels. In fact, an optimal coolant channel design using bifurcated HARCC was shown to not only reduce the T_{GW}, but to also provide a minimal reduction in the coolant channel pressure drop. Bifurcating channels does pose some manufacturing issues, such as in the transition areas. These result in the temperature spikes and some potential over cooling, as seen in Figure 20. However, these temperature spikes were minimized with an optimal bifurcated HARCC design, and the over cooling eliminated. Therefore, use of bifurcated high aspect ratio coolant channels is recommended if a reduction in T_{GW} is desired, with a minimal reduction in coolant pressure drop.

6. Concluding Remarks

The effect of high aspect ratio (height/width) cooling channels (HARCC) on hot-gas-side wall temperature (T_{GW}) and coolant pressure drop was analytically investigated, considering length of the HARCC, number of coolant channels, and coolant channel shape. The RTE and TDK codes were coupled to determine the T_{GW} and coolant pressure drop. First, the HARCC designs were determined without consideration for fabrication and produced T_{GW} reductions of 16.5 to 22 percent from the given baseline, with 7.5 to 33 percent increases in coolant pressure drop. The HARCC designs were then modified to reflect current milling fabrication techniques and limitations. The designs produced T_{GW} reductions of 8 to 20 percent from the given baseline, with 2 to 33 percent increases in coolant pressure drop. The fabrication constraints imposed did limit some of the designs in meeting the desired T_{GW}, however, a design was possible which was able to reduce the T_{GW} below the 667 K (1200 °R) limit without a severe coolant pressure drop penalty.

Using HARCC for the entire chamber length was shown to have no significant T_{GW} advantage over using HARCC only in the throat region, but did significantly increase the coolant pressure drop. Using 200 coolant channels for the entire chamber length was shown to benefit the T_{GW} profile, but would have a high coolant pressure drop penalty. All of the HARCC designs, once fabrication was considered, produced reductions in T_{GW} of at least 8 percent, with as little as a 2 percent increase in coolant pressure drop. Therefore, the use of HARCC was shown to have an overall benefit, independent of the coolant channel configurations investigated. The HARCC design which used bifurcated coolant channels had the most overall benefit with T_{GW} (20 percent reduction) and coolant pressure drop (9 percent increase). The bifurcated HARCC

design was then optimized, and was able to significantly reduce the T_{GW} (18 percent) and minimally reduce the coolant pressure drop (4 percent).

The effects of reduced coolant mass flow rate were investigated. Both the optimized design and design 5, which considered fabrication, were evaluated down to a 50 percent reduction in coolant mass flow rate, at 10 percent increments. At a 40 percent reduction in coolant mass flow rate, the optimized design was still able to produce a 5 percent reduction in T_{GW} and a 47 percent reduction in coolant pressure drop. Design 5, which considered fabrication, showed similar results. Therefore, if an optimized HARCC design is not possible, using bifurcated HARCC can still have a benefit to both the T_{GW} and coolant pressure drop by making reductions in the coolant mass flow rate.

This study showed that using bifurcated high aspect ratio channels gave enhanced cooling in the throat region due to the use of multiple coolant channels, but did not greatly increase the coolant pressure drop over a chamber which did not bifurcate the channels. It also showed that the coolant pressure drop could be reduced significantly with reductions in the coolant mass flow rate, and a reduction in T_{GW} could still be realized.

Appendix A - Coolant Channel Geometries for Each Design

Table A-I.—Coolant Channel Geometry for Design 1 Without Consideration
for Fabrication

Chamber Length (in)	Channel Width (in)	Channel Height (in)	Aspect Ratio	Landwidth (in)
3.208	0.035	0.179	5.102	0.177
2.872	0.035	0.179	5.102	0.164
2.009	0.035	0.179	5.102	0.129
1.719	0.035	0.179	5.102	0.117
1.464	0.033	0.182	5.510	0.107
1.347	0.031	0.185	5.983	0.104
1.135	0.029	0.190	6.540	0.096
1.038	0.028	0.188	6.696	0.093
0.947	0.027	0.148	5.487	0.090
0.778	0.025	0.160	6.400	0.084
0.701	0.023	0.174	7.561	0.082
0.452	0.020	0.200	10.000	0.073
0.250	0.015	0.267	17.778	0.072
0.100	0.012	0.333	27.778	0.072
0.000	0.010	0.400	40.000	0.074
-0.100	0.010	0.400	40.000	0.074
-0.274	0.010	0.400	40.000	0.076
-0.506	0.012	0.333	27.778	0.076
-0.906	0.016	0.328	20.508	0.078
-1.306	0.019	0.303	15.928	0.080
-1.706	0.025	0.240	9.600	0.080
-1.906	0.031	0.202	6.504	0.076
-2.106	0.033	0.189	5.739	0.077
-2.306	0.035	0.179	5.102	0.078
-2.506	0.035	0.179	5.102	0.080
-2.906	0.035	0.179	5.102	0.086
-3.106	0.035	0.179	5.102	0.088
-3.306	0.035	0.179	5.102	0.091
-3.506	0.035	0.179	5.102	0.094
-3.706	0.035	0.179	5.102	0.096
-3.906	0.035	0.179	5.102	0.098
-4.106	0.035	0.179	5.102	0.100
-4.506	0.035	0.179	5.102	0.104
-5.506	0.035	0.179	5.102	0.112
-5.906	0.035	0.179	5.102	0.114
-6.106	0.035	0.179	5.102	0.115
-6.506	0.035	0.179	5.102	0.116
-7.572	0.035	0.179	5.102	0.118
-8.350	0.035	0.179	5.102	0.118
-9.000	0.035	0.179	5.102	0.118
-9.375	0.035	0.179	5.102	0.118

Table A-II.—Coolant Channel Geometry for Design 2 Without Consideration
for Fabrication

Chamber Length (in)	Channel Width (in)	Channel Height (in)	Aspect Ratio	Landwidth (in)
3.208	0.025	0.125	5.000	0.081
2.872	0.025	0.125	5.000	0.075
2.009	0.025	0.125	5.000	0.057
1.719	0.025	0.125	5.000	0.051
1.464	0.025	0.120	4.800	0.045
1.347	0.024	0.120	4.991	0.043
1.135	0.023	0.120	5.198	0.040
1.038	0.023	0.114	4.962	0.037
0.947	0.020	0.100	5.000	0.038
0.778	0.020	0.100	5.000	0.034
0.701	0.020	0.100	5.000	0.032
0.452	0.020	0.100	5.000	0.027
0.250	0.020	0.100	5.000	0.023
0.100	0.020	0.100	5.000	0.022
0.000	0.020	0.100	5.000	0.022
-0.100	0.018	0.111	6.173	0.024
-0.274	0.018	0.111	6.173	0.025
-0.506	0.020	0.100	5.000	0.024
-0.906	0.023	0.114	4.962	0.024
-1.306	0.024	0.120	4.991	0.026
-1.706	0.025	0.120	4.800	0.027
-1.906	0.025	0.125	5.000	0.029
-2.106	0.025	0.125	5.000	0.030
-2.306	0.025	0.125	5.000	0.031
-2.506	0.025	0.125	5.000	0.033
-2.906	0.025	0.125	5.000	0.035
-3.106	0.025	0.125	5.000	0.037
-3.306	0.025	0.125	5.000	0.038
-3.506	0.025	0.125	5.000	0.039
-3.706	0.025	0.125	5.000	0.041
-3.906	0.025	0.125	5.000	0.042
-4.106	0.025	0.125	5.000	0.043
-4.506	0.025	0.125	5.000	0.045
-5.506	0.025	0.125	5.000	0.048
-5.906	0.025	0.125	5.000	0.049
-6.106	0.025	0.125	5.000	0.050
-6.506	0.025	0.125	5.000	0.051
-7.572	0.025	0.125	5.000	0.051
-8.350	0.025	0.125	5.000	0.051
-9.000	0.025	0.125	5.000	0.051
-9.375	0.025	0.125	5.000	0.051

Table A-III.—Coolant Channel Geometry for Design 3 Without Consideration for Fabrication

Chamber Length (in)	Channel Width (in)	Channel Height (in)	Aspect Ratio	Landwidth (in)
3.208	0.050	0.125	2.500	0.162
2.872	0.050	0.125	2.500	0.149
2.009	0.050	0.125	2.500	0.114
1.719	0.050	0.125	2.500	0.102
1.464	0.049	0.122	2.499	0.091
1.347	0.048	0.120	2.496	0.087
1.135	0.047	0.117	2.490	0.078
1.038	0.040	0.131	3.281	0.081
0.947	0.035	0.114	3.265	0.082
0.778	0.027	0.148	5.487	0.082
0.701	0.025	0.160	6.400	0.080
0.452	0.015	0.267	17.778	0.078
0.250	0.010	0.400	40.000	0.077
0.100	0.010	0.400	40.000	0.074
0.000	0.010	0.400	40.000	0.074
-0.100	0.010	0.400	40.000	0.074
-0.274	0.010	0.400	40.000	0.076
-0.506	0.012	0.333	27.778	0.076
-0.906	0.015	0.350	23.333	0.079
-1.306	0.020	0.288	14.375	0.079
-1.706	0.028	0.214	7.653	0.077
-1.906	0.035	0.179	5.102	0.072
-2.106	0.040	0.156	3.906	0.070
-2.306	0.045	0.139	3.086	0.068
-2.506	0.050	0.125	2.500	0.065
-2.906	0.050	0.125	2.500	0.071
-3.106	0.050	0.125	2.500	0.073
-3.306	0.050	0.125	2.500	0.076
-3.506	0.050	0.125	2.500	0.079
-3.706	0.050	0.125	2.500	0.081
-3.906	0.050	0.125	2.500	0.083
-4.106	0.050	0.125	2.500	0.085
-4.506	0.050	0.125	2.500	0.089
-5.506	0.050	0.125	2.500	0.097
-5.906	0.050	0.125	2.500	0.099
-6.106	0.050	0.125	2.500	0.100
-6.506	0.050	0.125	2.500	0.101
-7.572	0.050	0.125	2.500	0.103
-8.350	0.050	0.125	2.500	0.103
-9.000	0.050	0.125	2.500	0.103
-9.375	0.050	0.125	2.500	0.103

Table A-IV.—Coolant Channel Geometry for Design 4 Without Consideration for Fabrication

Chamber Length (in)	Channel Width (in)	Channel Height (in)	Aspect Ratio	Landwidth (in)
3.208	0.035	0.089	2.551	0.071
2.872	0.035	0.089	2.551	0.065
2.009	0.035	0.089	2.551	0.047
1.719	0.035	0.089	2.551	0.041
1.464	0.034	0.088	2.595	0.036
1.347	0.034	0.085	2.487	0.033
1.135	0.033	0.083	2.525	0.030
1.038	0.033	0.080	2.410	0.027
0.947	0.030	0.067	2.222	0.028
0.778	0.025	0.080	3.200	0.029
0.701	0.020	0.100	5.000	0.032
0.452	0.020	0.100	5.000	0.027
0.250	0.020	0.100	5.000	0.023
0.100	0.020	0.100	5.000	0.022
0.000	0.020	0.100	5.000	0.022
-0.100	0.020	0.100	5.000	0.022
-0.274	0.020	0.100	5.000	0.023
-0.506	0.024	0.083	3.472	0.020
-0.906	0.028	0.094	3.348	0.019
-1.306	0.030	0.096	3.194	0.020
-1.706	0.035	0.086	2.449	0.017
-1.906	0.035	0.089	2.551	0.019
-2.106	0.035	0.089	2.551	0.020
-2.306	0.035	0.089	2.551	0.021
-2.506	0.035	0.089	2.551	0.023
-2.906	0.035	0.089	2.551	0.025
-3.106	0.035	0.089	2.551	0.027
-3.306	0.035	0.089	2.551	0.028
-3.506	0.035	0.089	2.551	0.029
-3.706	0.035	0.089	2.551	0.031
-3.906	0.035	0.089	2.551	0.032
-4.106	0.035	0.089	2.551	0.033
-4.506	0.035	0.089	2.551	0.035
-5.506	0.035	0.089	2.551	0.038
-5.906	0.035	0.089	2.551	0.039
-6.106	0.035	0.089	2.551	0.040
-6.506	0.035	0.089	2.551	0.041
-7.572	0.035	0.089	2.551	0.041
-8.350	0.035	0.089	2.551	0.041
-9.000	0.035	0.089	2.551	0.041
-9.375	0.035	0.089	2.551	0.041

Table A-V.—Coolant Channel Geometry for Design 5 Without Consideration
for Fabrication

Chamber Length (in)	Channel Width (in)	Channel Height (in)	Aspect Ratio	Landwidth (in)
3.208	0.050	0.125	2.500	0.162
2.872	0.050	0.125	2.500	0.149
2.009	0.050	0.125	2.500	0.114
1.719	0.050	0.125	2.500	0.102
1.464	0.050	0.120	2.400	0.090
1.347	0.050	0.115	2.300	0.085
1.135	0.050	0.110	2.200	0.075
1.038	0.045	0.117	2.593	0.076
0.947	0.043	0.093	2.163	0.074
0.778	0.040	0.100	2.500	0.069
0.701	0.035	0.057	1.633	0.017
0.452	0.030	0.067	2.222	0.017
0.250	0.025	0.080	3.200	0.018
0.100	0.020	0.100	5.000	0.022
0.000	0.020	0.100	5.000	0.022
-0.100	0.020	0.100	5.000	0.022
-0.274	0.020	0.100	5.000	0.023
-0.506	0.025	0.080	3.200	0.019
-0.906	0.029	0.091	3.121	0.018
-1.306	0.030	0.096	3.194	0.020
-1.706	0.026	0.231	8.876	0.079
-1.906	0.032	0.195	6.104	0.075
-2.106	0.037	0.169	4.565	0.073
-2.306	0.045	0.139	3.086	0.068
-2.506	0.050	0.125	2.500	0.065
-2.906	0.050	0.125	2.500	0.071
-3.106	0.050	0.125	2.500	0.073
-3.306	0.050	0.125	2.500	0.076
-3.506	0.050	0.125	2.500	0.079
-3.706	0.050	0.125	2.500	0.081
-3.906	0.050	0.125	2.500	0.083
-4.106	0.050	0.125	2.500	0.085
-4.506	0.050	0.125	2.500	0.089
-5.506	0.050	0.125	2.500	0.097
-5.906	0.050	0.125	2.500	0.099
-6.106	0.050	0.125	2.500	0.100
-6.506	0.050	0.125	2.500	0.101
-7.572	0.050	0.125	2.500	0.103
-8.350	0.050	0.125	2.500	0.103
-9.000	0.050	0.125	2.500	0.103
-9.375	0.050	0.125	2.500	0.103

Table A-VI.—Coolant Channel Geometry for Design 6 Without Consideration
for Fabrication

Chamber Length (in)	Channel Width (in)	Channel Height (in)	Aspect Ratio	Landwidth (in)
3.208	0.050	0.125	2.500	0.162
2.872	0.050	0.125	2.500	0.149
2.009	0.050	0.125	2.500	0.114
1.719	0.050	0.125	2.500	0.102
1.464	0.050	0.120	2.400	0.090
1.347	0.050	0.115	2.300	0.085
1.135	0.050	0.110	2.200	0.075
1.038	0.050	0.105	2.100	0.071
0.947	0.040	0.100	2.500	0.077
0.778	0.040	0.100	2.500	0.069
0.701	0.040	0.100	2.500	0.065
0.452	0.040	0.100	2.500	0.053
0.250	0.010	0.400	40.000	0.077
0.100	0.010	0.400	40.000	0.074
0.000	0.010	0.400	40.000	0.074
-0.100	0.010	0.400	40.000	0.074
-0.274	0.010	0.400	40.000	0.076
-0.506	0.010	0.400	40.000	0.078
-0.906	0.015	0.350	23.333	0.079
-1.306	0.015	0.383	25.556	0.084
-1.706	0.030	0.200	6.667	0.075
-1.906	0.030	0.208	6.944	0.077
-2.106	0.030	0.208	6.944	0.080
-2.306	0.030	0.208	6.944	0.083
-2.506	0.050	0.125	2.500	0.065
-2.906	0.050	0.125	2.500	0.071
-3.106	0.050	0.125	2.500	0.073
-3.306	0.050	0.125	2.500	0.076
-3.506	0.050	0.125	2.500	0.079
-3.706	0.050	0.125	2.500	0.081
-3.906	0.050	0.125	2.500	0.083
-4.106	0.050	0.125	2.500	0.085
-4.506	0.050	0.125	2.500	0.089
-5.506	0.050	0.125	2.500	0.097
-5.906	0.050	0.125	2.500	0.099
-6.106	0.050	0.125	2.500	0.100
-6.506	0.050	0.125	2.500	0.101
-7.572	0.050	0.125	2.500	0.103
-8.350	0.050	0.125	2.500	0.103
-9.000	0.050	0.125	2.500	0.103
-9.375	0.050	0.125	2.500	0.103

Table A-VII.—Coolant Channel Geometry for Design 7 Without Consideration for Fabrication

Chamber Length (in)	Channel Width (in)	Channel Height (in)	Aspect Ratio	Landwidth (in)
3.208	0.035	0.089	2.551	0.071
2.872	0.035	0.089	2.551	0.065
2.009	0.035	0.089	2.551	0.047
1.719	0.035	0.089	2.551	0.041
1.464	0.035	0.086	2.449	0.035
1.347	0.035	0.082	2.347	0.032
1.135	0.035	0.079	2.245	0.028
1.038	0.035	0.075	2.143	0.025
0.947	0.020	0.100	5.000	0.038
0.778	0.020	0.100	5.000	0.034
0.701	0.020	0.100	5.000	0.032
0.452	0.020	0.100	5.000	0.027
0.250	0.020	0.100	5.000	0.023
0.100	0.020	0.100	5.000	0.022
0.000	0.020	0.100	5.000	0.022
-0.100	0.018	0.111	6.173	0.024
-0.274	0.018	0.111	6.173	0.025
-0.506	0.018	0.111	6.173	0.026
-0.906	0.025	0.105	4.200	0.022
-1.306	0.025	0.115	4.600	0.025
-1.706	0.035	0.086	2.449	0.017
-1.906	0.035	0.089	2.551	0.019
-2.106	0.035	0.089	2.551	0.020
-2.306	0.035	0.089	2.551	0.021
-2.506	0.035	0.089	2.551	0.023
-2.906	0.035	0.089	2.551	0.025
-3.106	0.035	0.089	2.551	0.027
-3.306	0.035	0.089	2.551	0.028
-3.506	0.035	0.089	2.551	0.029
-3.706	0.035	0.089	2.551	0.031
-3.906	0.035	0.089	2.551	0.032
-4.106	0.035	0.089	2.551	0.033
-4.506	0.035	0.089	2.551	0.035
-5.506	0.035	0.089	2.551	0.038
-5.906	0.035	0.089	2.551	0.039
-6.106	0.035	0.089	2.551	0.040
-6.506	0.035	0.089	2.551	0.041
-7.572	0.035	0.089	2.551	0.041
-8.350	0.035	0.089	2.551	0.041
-9.000	0.035	0.089	2.551	0.041
-9.375	0.035	0.089	2.551	0.041

Table A-VIII.—Coolant Channel Geometry for Design 1 Considering Fabrication

Chamber Length (in)	Channel Width (in)	Channel Height (in)	Aspect Ratio	Landwidth (in)
3.208	0.035	0.179	5.102	0.177
2.872	0.035	0.179	5.102	0.164
2.009	0.035	0.179	5.102	0.129
1.719	0.035	0.179	5.102	0.117
1.464	0.033	0.182	5.510	0.107
1.347	0.031	0.185	5.983	0.104
1.135	0.030	0.183	6.111	0.095
1.038	0.029	0.181	6.243	0.092
0.947	0.023	0.174	7.561	0.094
0.778	0.023	0.174	7.561	0.086
0.701	0.023	0.174	7.561	0.082
0.452	0.023	0.174	7.561	0.070
0.250	0.023	0.174	7.561	0.064
0.100	0.023	0.174	7.561	0.061
0.000	0.023	0.174	7.561	0.061
-0.100	0.023	0.174	7.561	0.061
-0.274	0.023	0.174	7.561	0.063
-0.506	0.023	0.174	7.561	0.065
-0.906	0.027	0.194	7.202	0.067
-1.306	0.029	0.198	6.837	0.070
-1.706	0.030	0.200	6.667	0.075
-1.906	0.032	0.195	6.104	0.075
-2.106	0.032	0.195	6.104	0.078
-2.306	0.035	0.179	5.102	0.078
-2.506	0.035	0.179	5.102	0.080
-2.906	0.035	0.179	5.102	0.086
-3.106	0.035	0.179	5.102	0.088
-3.306	0.035	0.179	5.102	0.091
-3.506	0.035	0.179	5.102	0.094
-3.706	0.035	0.179	5.102	0.096
-3.906	0.035	0.179	5.102	0.098
-4.106	0.035	0.179	5.102	0.100
-4.506	0.035	0.179	5.102	0.104
-5.506	0.035	0.179	5.102	0.112
-5.906	0.035	0.179	5.102	0.114
-6.106	0.035	0.179	5.102	0.115
-6.506	0.035	0.179	5.102	0.116
-7.572	0.035	0.179	5.102	0.118
-8.350	0.035	0.179	5.102	0.118
-9.000	0.035	0.179	5.102	0.118
-9.375	0.035	0.179	5.102	0.118

Table A-IX.—Coolant Channel Geometry for Design 2 Considering Fabrication

Chamber Length (in)	Channel Width (in)	Channel Height (in)	Aspect Ratio	Landwidth (in)
3.208	0.025	0.125	5.000	0.081
2.872	0.025	0.125	5.000	0.075
2.009	0.025	0.125	5.000	0.057
1.719	0.025	0.125	5.000	0.051
1.464	0.025	0.120	4.800	0.045
1.347	0.024	0.120	4.991	0.043
1.135	0.023	0.120	5.198	0.040
1.038	0.023	0.114	4.962	0.037
0.947	0.020	0.100	5.000	0.038
0.778	0.020	0.100	5.000	0.034
0.701	0.020	0.100	5.000	0.032
0.452	0.020	0.100	5.000	0.027
0.250	0.020	0.100	5.000	0.023
0.100	0.020	0.100	5.000	0.022
0.000	0.020	0.100	5.000	0.022
-0.100	0.020	0.100	5.000	0.022
-0.274	0.020	0.100	5.000	0.023
-0.506	0.020	0.100	5.000	0.024
-0.906	0.023	0.114	4.962	0.024
-1.306	0.024	0.120	4.991	0.026
-1.706	0.025	0.120	4.800	0.027
-1.906	0.025	0.125	5.000	0.029
-2.106	0.025	0.125	5.000	0.030
-2.306	0.025	0.125	5.000	0.031
-2.506	0.025	0.125	5.000	0.033
-2.906	0.025	0.125	5.000	0.035
-3.106	0.025	0.125	5.000	0.037
-3.306	0.025	0.125	5.000	0.038
-3.506	0.025	0.125	5.000	0.039
-3.706	0.025	0.125	5.000	0.041
-3.906	0.025	0.125	5.000	0.042
-4.106	0.025	0.125	5.000	0.043
-4.506	0.025	0.125	5.000	0.045
-5.506	0.025	0.125	5.000	0.048
-5.906	0.025	0.125	5.000	0.049
-6.106	0.025	0.125	5.000	0.050
-6.506	0.025	0.125	5.000	0.051
-7.572	0.025	0.125	5.000	0.051
-8.350	0.025	0.125	5.000	0.051
-9.000	0.025	0.125	5.000	0.051
-9.375	0.025	0.125	5.000	0.051

Table A-X.—Coolant Channel Geometry for Design 3 Considering Fabrication

Chamber Length (in)	Channel Width (in)	Channel Height (in)	Aspect Ratio	Landwidth (in)
3.208	0.050	0.125	2.500	0.162
2.872	0.050	0.125	2.500	0.149
2.009	0.050	0.125	2.500	0.114
1.719	0.049	0.128	2.603	0.103
1.464	0.045	0.133	2.963	0.095
1.347	0.040	0.144	3.594	0.095
1.135	0.035	0.157	4.490	0.090
1.038	0.032	0.164	5.127	0.089
0.947	0.026	0.154	5.917	0.091
0.778	0.023	0.174	7.561	0.086
0.701	0.023	0.174	7.561	0.082
0.452	0.023	0.174	7.561	0.070
0.250	0.023	0.174	7.561	0.064
0.100	0.023	0.174	7.561	0.061
0.000	0.023	0.174	7.561	0.061
-0.100	0.023	0.174	7.561	0.061
-0.274	0.023	0.174	7.561	0.063
-0.506	0.023	0.174	7.561	0.065
-0.906	0.027	0.194	7.202	0.067
-1.306	0.029	0.198	6.837	0.070
-1.706	0.030	0.200	6.667	0.075
-1.906	0.033	0.189	5.739	0.074
-2.106	0.035	0.179	5.102	0.075
-2.306	0.040	0.156	3.906	0.073
-2.506	0.045	0.139	3.086	0.070
-2.906	0.050	0.125	2.500	0.071
-3.106	0.050	0.125	2.500	0.073
-3.306	0.050	0.125	2.500	0.076
-3.506	0.050	0.125	2.500	0.079
-3.706	0.050	0.125	2.500	0.081
-3.906	0.050	0.125	2.500	0.083
-4.106	0.050	0.125	2.500	0.085
-4.506	0.050	0.125	2.500	0.089
-5.506	0.050	0.125	2.500	0.097
-5.906	0.050	0.125	2.500	0.099
-6.106	0.050	0.125	2.500	0.100
-6.506	0.050	0.125	2.500	0.101
-7.572	0.050	0.125	2.500	0.103
-8.350	0.050	0.125	2.500	0.103
-9.000	0.050	0.125	2.500	0.103
-9.375	0.050	0.125	2.500	0.103

Table A-XI.—Coolant Channel Geometry for Design 4 Considering Fabrication

Chamber Length (in)	Channel Width (in)	Channel Height (in)	Aspect Ratio	Landwidth (in)
3.208	0.035	0.089	2.551	0.071
2.872	0.035	0.089	2.551	0.065
2.009	0.035	0.089	2.551	0.047
1.719	0.035	0.089	2.551	0.041
1.464	0.034	0.088	2.595	0.036
1.347	0.034	0.085	2.487	0.033
1.135	0.033	0.083	2.525	0.030
1.038	0.032	0.082	2.563	0.028
0.947	0.026	0.077	2.959	0.032
0.778	0.024	0.083	3.472	0.030
0.701	0.023	0.087	3.781	0.029
0.452	0.020	0.100	5.000	0.027
0.250	0.020	0.100	5.000	0.023
0.100	0.020	0.100	5.000	0.022
0.000	0.020	0.100	5.000	0.022
-0.100	0.020	0.100	5.000	0.022
-0.274	0.020	0.100	5.000	0.023
-0.506	0.022	0.091	4.132	0.022
-0.906	0.027	0.097	3.601	0.020
-1.306	0.030	0.096	3.194	0.020
-1.706	0.032	0.094	2.930	0.020
-1.906	0.034	0.092	2.703	0.020
-2.106	0.035	0.089	2.551	0.020
-2.306	0.035	0.089	2.551	0.021
-2.506	0.035	0.089	2.551	0.023
-2.906	0.035	0.089	2.551	0.025
-3.106	0.035	0.089	2.551	0.027
-3.306	0.035	0.089	2.551	0.028
-3.506	0.035	0.089	2.551	0.029
-3.706	0.035	0.089	2.551	0.031
-3.906	0.035	0.089	2.551	0.032
-4.106	0.035	0.089	2.551	0.033
-4.506	0.035	0.089	2.551	0.035
-5.506	0.035	0.089	2.551	0.038
-5.906	0.035	0.089	2.551	0.039
-6.106	0.035	0.089	2.551	0.040
-6.506	0.035	0.089	2.551	0.041
-7.572	0.035	0.089	2.551	0.041
-8.350	0.035	0.089	2.551	0.041
-9.000	0.035	0.089	2.551	0.041
-9.375	0.035	0.089	2.551	0.041

Table A-XII.—Coolant Channel Geometry for Design 5 Considering Fabrication

Chamber Length (in)	Channel Width (in)	Channel Height (in)	Aspect Ratio	Landwidth (in)
3.208	0.050	0.125	2.500	0.162
2.872	0.050	0.125	2.500	0.149
2.009	0.050	0.125	2.500	0.114
1.719	0.050	0.125	2.500	0.102
1.464	0.050	0.120	2.400	0.090
1.347	0.053	0.108	2.047	0.082
1.135	0.057	0.110	1.924	0.068
1.038	0.062	0.107	1.730	0.059
0.947	0.066	0.104	1.579	0.051
0.778	0.070	0.100	1.429	0.039
0.701	0.022	0.091	4.132	0.030
0.452	0.021	0.095	4.535	0.026
0.250	0.020	0.100	5.000	0.023
0.100	0.020	0.100	5.000	0.022
0.000	0.020	0.100	5.000	0.022
-0.100	0.020	0.100	5.000	0.022
-0.274	0.020	0.100	5.000	0.023
-0.506	0.020	0.100	5.000	0.024
-0.906	0.025	0.105	4.200	0.022
-1.306	0.027	0.106	3.944	0.023
-1.706	0.028	0.107	3.827	0.024
-1.906	0.030	0.104	3.472	0.024
-2.106	0.030	0.104	3.472	0.025
-2.306	0.030	0.104	3.472	0.026
-2.506	0.030	0.104	3.472	0.028
-2.906	0.030	0.104	3.472	0.030
-3.106	0.030	0.104	3.472	0.032
-3.306	0.030	0.104	3.472	0.033
-3.506	0.030	0.104	3.472	0.034
-3.706	0.030	0.104	3.472	0.036
-3.906	0.030	0.104	3.472	0.037
-4.106	0.075	0.111	1.476	0.060
-4.506	0.055	0.118	2.149	0.084
-5.506	0.050	0.125	2.500	0.097
-5.906	0.050	0.125	2.500	0.099
-6.106	0.050	0.125	2.500	0.100
-6.506	0.050	0.125	2.500	0.101
-7.572	0.050	0.125	2.500	0.103
-8.350	0.050	0.125	2.500	0.103
-9.000	0.050	0.125	2.500	0.103
-9.375	0.050	0.125	2.500	0.103

Table A-XIII.—Coolant Channel Geometry for Design 6 Considering Fabrication

Chamber Length (in)	Channel Width (in)	Channel Height (in)	Aspect Ratio	Landwidth (in)
3.208	0.050	0.125	2.500	0.162
2.872	0.050	0.125	2.500	0.149
2.009	0.050	0.125	2.500	0.114
1.719	0.050	0.125	2.500	0.102
1.464	0.050	0.120	2.400	0.090
1.347	0.050	0.115	2.300	0.085
1.135	0.050	0.110	2.200	0.075
1.038	0.050	0.105	2.100	0.071
0.947	0.040	0.100	2.500	0.077
0.778	0.040	0.100	2.500	0.069
0.701	0.040	0.100	2.500	0.065
0.452	0.040	0.100	2.500	0.053
0.250	0.023	0.174	7.561	0.064
0.100	0.023	0.174	7.561	0.061
0.000	0.023	0.174	7.561	0.061
-0.100	0.023	0.174	7.561	0.061
-0.274	0.023	0.174	7.561	0.063
-0.506	0.023	0.174	7.561	0.065
-0.906	0.032	0.164	5.127	0.062
-1.306	0.032	0.180	5.615	0.067
-1.706	0.032	0.188	5.859	0.073
-1.906	0.032	0.195	6.104	0.075
-2.106	0.032	0.195	6.104	0.078
-2.306	0.032	0.195	6.104	0.081
-2.506	0.050	0.125	2.500	0.065
-2.906	0.050	0.125	2.500	0.071
-3.106	0.050	0.125	2.500	0.073
-3.306	0.050	0.125	2.500	0.076
-3.506	0.050	0.125	2.500	0.079
-3.706	0.050	0.125	2.500	0.081
-3.906	0.050	0.125	2.500	0.083
-4.106	0.050	0.125	2.500	0.085
-4.506	0.050	0.125	2.500	0.089
-5.506	0.050	0.125	2.500	0.097
-5.906	0.050	0.125	2.500	0.099
-6.106	0.050	0.125	2.500	0.100
-6.506	0.050	0.125	2.500	0.101
-7.572	0.050	0.125	2.500	0.103
-8.350	0.050	0.125	2.500	0.103
-9.000	0.050	0.125	2.500	0.103
-9.375	0.050	0.125	2.500	0.103

Table A-XIV.—Coolant Channel Geometry for Design 7 Considering Fabrication

Chamber Length (in)	Channel Width (in)	Channel Height (in)	Aspect Ratio	Landwidth (in)
3.208	0.035	0.089	2.551	0.071
2.872	0.035	0.089	2.551	0.065
2.009	0.035	0.089	2.551	0.047
1.719	0.035	0.089	2.551	0.041
1.464	0.035	0.086	2.449	0.035
1.347	0.035	0.082	2.347	0.032
1.135	0.035	0.079	2.245	0.028
1.038	0.035	0.075	2.143	0.025
0.947	0.020	0.100	5.000	0.038
0.778	0.020	0.100	5.000	0.034
0.701	0.020	0.100	5.000	0.032
0.452	0.020	0.100	5.000	0.027
0.250	0.020	0.100	5.000	0.023
0.100	0.020	0.100	5.000	0.022
0.000	0.020	0.100	5.000	0.022
-0.100	0.020	0.100	5.000	0.022
-0.274	0.020	0.100	5.000	0.023
-0.506	0.020	0.100	5.000	0.024
-0.906	0.027	0.097	3.601	0.020
-1.306	0.027	0.106	3.944	0.023
-1.706	0.032	0.094	2.930	0.020
-1.906	0.032	0.098	3.052	0.022
-2.106	0.035	0.089	2.551	0.020
-2.306	0.035	0.089	2.551	0.021
-2.506	0.035	0.089	2.551	0.023
-2.906	0.035	0.089	2.551	0.025
-3.106	0.035	0.089	2.551	0.027
-3.306	0.035	0.089	2.551	0.028
-3.506	0.035	0.089	2.551	0.029
-3.706	0.035	0.089	2.551	0.031
-3.906	0.035	0.089	2.551	0.032
-4.106	0.035	0.089	2.551	0.033
-4.506	0.035	0.089	2.551	0.035
-5.506	0.035	0.089	2.551	0.038
-5.906	0.035	0.089	2.551	0.039
-6.106	0.035	0.089	2.551	0.040
-6.506	0.035	0.089	2.551	0.041
-7.572	0.035	0.089	2.551	0.041
-8.350	0.035	0.089	2.551	0.041
-9.000	0.035	0.089	2.551	0.041
-9.375	0.035	0.089	2.551	0.041

Table A-XV.—Coolant Channel Geometry for Design 5 Optimized.

Chamber Length (in)	Channel Width (in)	Channel Height (in)	Aspect Ratio	Landwidth (in)
3.208	0.050	0.125	2.500	0.162
2.872	0.050	0.125	2.500	0.149
2.009	0.050	0.125	2.500	0.114
1.719	0.050	0.125	2.500	0.102
1.464	0.050	0.120	2.400	0.090
1.347	0.053	0.115	2.170	0.082
1.135	0.057	0.110	1.930	0.068
1.038	0.062	0.108	1.742	0.059
0.947	0.066	0.105	1.591	0.051
0.778	0.070	0.100	1.429	0.039
0.701	0.025	0.100	4.000	0.027
0.452	0.022	0.100	4.545	0.025
0.250	0.020	0.100	5.000	0.023
0.100	0.020	0.100	5.000	0.022
0.000	0.020	0.100	5.000	0.022
-0.100	0.020	0.100	5.000	0.022
-0.274	0.020	0.100	5.000	0.023
-0.506	0.022	0.100	4.545	0.022
-0.906	0.027	0.100	3.704	0.020
-1.306	0.029	0.105	3.621	0.021
-1.706	0.032	0.117	3.656	0.020
-1.906	0.034	0.124	3.647	0.020
-2.106	0.035	0.130	3.714	0.020
-2.306	0.036	0.137	3.806	0.020
-2.506	0.038	0.137	3.605	0.020
-2.906	0.040	0.125	3.125	0.020
-3.106	0.041	0.125	3.049	0.021
-3.306	0.043	0.123	2.860	0.020
-3.506	0.044	0.120	2.727	0.020
-3.706	0.045	0.118	2.622	0.021
-3.906	0.045	0.116	2.578	0.022
-4.106	0.075	0.115	1.643	0.065
-4.506	0.055	0.120	2.182	0.084
-5.506	0.050	0.125	2.500	0.097
-5.906	0.050	0.125	2.500	0.099
-6.106	0.050	0.125	2.500	0.100
-6.506	0.050	0.125	2.500	0.101
-7.572	0.050	0.125	2.500	0.103
-8.350	0.050	0.125	2.500	0.103
-9.000	0.050	0.125	2.500	0.103
-9.375	0.050	0.125	2.500	0.103

References

1. Carlile, J.A., Quentmeyer, R.J.: An Experimental Investigation of High-Aspect-Ratio Cooling Passages, 28th Joint Propulsion Conference, 1992, AIAA-92-3154 (Also NASA TM-105679).

2. Wadel, M.F., Meyer, M.L.: Validation of High Aspect Ratio Cooling in a 89 kN (20,000 lbf) Thrust Combustion Chamber, 32nd Joint Propulsion Conference, 1996, AIAA-96-2584 (Also NASA TM-107270).

3. Incropera, F.P., DeWitt, D.P.: Fundamentals of Heat and Mass Transfer, John Wiley & Sons, Inc., New York, NY, 1981.

4. Wadel, M.F., Quentmeyer, R.J., Meyer, M.L.: A Rocket Engine Design for Validating the High Aspect Ratio Cooling Channel Concept, NASA Conference Publication 3282, Vol. II, pp. 145-150, 1994.

5. Muss, J.A., Nguyen, T.V., Johnson, C.W.: User's Manual for Rocket Combustor Interactive Design (ROCCID) and Analysis Computer Program, NASA Contractor Report 187109, Contract NAS3-25556, May 1991.

6. Naraghi, M.H.N.: User's Manual, RTE - A Computer Code for Three-Dimensional Rocket Thermal Evaluation, Manhattan College, Riverdale, NY September 1993, under NASA grant NAG 3-892.

7. Nickerson, G.R., Coats, D.E., Dang, A.L., Dunn, S.S., Kehtarnavaz, H.: Two-Dimensional Kinetics (TDK) Nozzle Performance Computer Program, NAS8-36863, March 1989.

8. Gordon, S., McBride, B.J.: Computer Program for Calculation of Complex Chemical Equilibrium Compositions, Rocket Performance, Incident and Reflection Shocks, and Chapman-Jouquet Detonations, NASA SP-270, 1971.

9. Gordon, S., McBride, B.J., Zeleznick, F.J.: Computer Program for Calculation of Complex Chemical Equilibrium Compositions and Applications Supplement I - Transport Properties, NASA TM-86885, October 1984.

10. Hendricks, R.C., Baron, A.K., Peller, I.C.: GASP - A Computer Code for Calculating the Thermodynamic and Transport Properties for Ten Fluids: Parahydrogen, Helium, Neon, Methane, Nitrogen, Carbon Monoxide, Oxygen, Fluorine, Argon, and Carbon Dioxide, NASA TN D-7808, February 1975.

11. Eckert, E.R.G., Drake, R.M.: Analysis of Heat and Mass Transfer, McGraw-Hill Book Company, 1972.

12. Bartz, D.R.: Turbulent Boundary-Layer Heat Transfer from Rapidly Accelerating Flow of Rocket Combustion Gases and of Heated Air, Advances in Heat Transfer, pp. 2-108, 1965.

13. Niino, M., Kumakawa, A., Yatsuyanagi, N., Suzuki, A.: Heat Transfer Characteristics of Liquid Hydrogen as a Coolant for the LO2/LH2 Rocket Thrust Chamber with the Channel Wall Construction, 18th AIAA/SAE/ASME Joint Propulsion Conference, Cleveland, Ohio, June 21-23, 1982, AIAA Paper 82-1107.

14. Owhadi, A., Bell, K.J., Crain, B.: Forced Convection Boiling Inside Helically-Coiled Tubes, International Journal of Heat and Mass Transfer, Vol. 11, pp. 1779-1793, 1968.

15. Chen, N.H.: An Explicit Equation for Friction Factor in Pipe, Ind. Eng. Chem. Fundam., Vol. 18, No. 3, pp. 296-297, 1979.

16. Ito, H.: Friction Factors for Turbulent Flow in Curved Pipes, Journal of Basic Engineering, pp. 123-134, 1959.

17. Moody, L.F.: Friction Factors for Pipe Flow, Transactions of ASME, pp. 671-684, 1944.

18. Keller, H.B., Cebeci, T.: Accurate Numerical Methods for Boundary-Layer Flows. II: Two Dimensional Turbulent Flows, AIAA J., Vol. 10, No. 9, Sept. 1972, p. 1193-1199.

19. Cebeci, T., Smith, A.M.O.: Analysis of Turbulent Boundary Layers, Academic Press, 1974.

20. Kacynski, K.J.: Thermal Stratification Potential in Rocket Engine Coolant Channels, NASA TM-4378, Presented at the JANNAF Propulsion Meeting, Vol. 1, pp. 329-338, 1992.

21. Meyer, M.L., Giuliani, J.E.: Visualization of Secondary Flow Development in High Aspect Ratio Channels with Curvature, AIAA-94-2979, NASA TM-106658, 1994.

22. Meyer, M.L.: Electrically Heated Tube Investigation of Cooling Channel Geometry Effects, AIAA-95-2500, NASA TM-106985, 1995.

23. Meyer, M.L.: The Effect of Cooling Passage Aspect Ratio on Curvature Heat Transfer Enhancement, NASA TM-107426, 1997.

24. Yagley, J., Feng, J., Merkle, C.L., Lee, Y.-T.: The Effect of Aspect Ratio on the Effectiveness of Combustor Coolant Passages, 28th Joint Propulsion Conference, 1992, AIAA-92-3153.

25. Quentmeyer, R.J.: Experimental Fatigue Life Investigation of Cylindrical Thrust Chambers, 13th Propulsion Conference, 1977, NASA TM X-73665.

REPORT DOCUMENTATION PAGE

1. AGENCY USE ONLY (Leave blank)	2. REPORT DATE	3. REPORT TYPE AND DATES COVERED
	January 1998	Technical Memorandum

4. TITLE AND SUBTITLE

Comparison of High Aspect Ratio Cooling Channel Designs for a Rocket Combustion Chamber With Development of an Optimized Design

5. FUNDING NUMBERS

WU–242-72-01-00

6. AUTHOR(S)

Mary F. Wadel

7. PERFORMING ORGANIZATION NAME(S) AND ADDRESS(ES)

National Aeronautics and Space Administration
Lewis Research Center
Cleveland, Ohio 44135–3191

8. PERFORMING ORGANIZATION REPORT NUMBER

E–10996

9. SPONSORING/MONITORING AGENCY NAME(S) AND ADDRESS(ES)

National Aeronautics and Space Administration
Washington, DC 20546–0001

10. SPONSORING/MONITORING AGENCY REPORT NUMBER

NASA TM—1998-206313

11. SUPPLEMENTARY NOTES

12a. DISTRIBUTION/AVAILABILITY STATEMENT

Unclassified - Unlimited
Subject Categories: 20 and 34

Distribution: Nonstandard

This publication is available from the NASA Center for AeroSpace Information, (301) 621–0390.

12b. DISTRIBUTION CODE

13. ABSTRACT (Maximum 200 words)

An analytical investigation on the effect of high aspect ratio (height/width) cooling channels, considering different coolant channel designs, on hot-gas-side wall temperature and coolant pressure drop for a liquid hydrogen cooled rocket combustion chamber, was performed. Coolant channel design elements considered were; length of combustion chamber in which high aspect ratio cooling was applied, number of coolant channels, and coolant channel shape. Seven coolant channel designs were investigated using a coupling of the Rocket Thermal Evaluation code and the Two-Dimensional Kinetics code. Initially, each coolant channel design was developed, without consideration for fabrication, to reduce the hot-gas-side wall temperature from a given conventional cooling channel baseline. These designs produced hot-gas-side wall temperature reductions up to 22 percent, with coolant pressure drop increases as low as 7.5 percent from the baseline. Fabrication constraints for milled channels were applied to the seven designs. These produced hot-gas-side wall temperature reductions of up to 20 percent, with coolant pressure drop increases as low as 2 percent. Using high aspect ratio cooling channels for the entire length of the combustion chamber had no additional benefit on hot-gas-side wall temperature over using high aspect ratio cooling channels only in the throat region, but increased coolant pressure drop 33 percent. Independent of coolant channel shape, high aspect ratio cooling was able to reduce the hot-gas-side wall temperature by at least 8 percent, with as low as a 2 percent increase in coolant pressure drop. The design with the highest overall benefit to hot-gas-side wall temperature and minimal coolant pressure drop increase was the design which used bifurcated cooling channels and high aspect ratio cooling in the throat region. An optimized bifurcated high aspect ratio cooling channel design was developed which reduced the hot-gas-side wall temperature by 18 percent and reduced the coolant pressure drop by 4 percent. Reductions of coolant mass flow rate of up to 50 percent were possible before the hot-gas-side wall temperature reached that of the baseline. These mass flow rate reductions produced coolant pressure drops of up to 57 percent.

14. SUBJECT TERMS

Rocket combustors; Rocket Engine; Aspect ratio; Chamber liner

15. NUMBER OF PAGES

80

16. PRICE CODE

A05

17. SECURITY CLASSIFICATION OF REPORT	18. SECURITY CLASSIFICATION OF THIS PAGE	19. SECURITY CLASSIFICATION OF ABSTRACT	20. LIMITATION OF ABSTRACT
Unclassified	Unclassified	Unclassified	